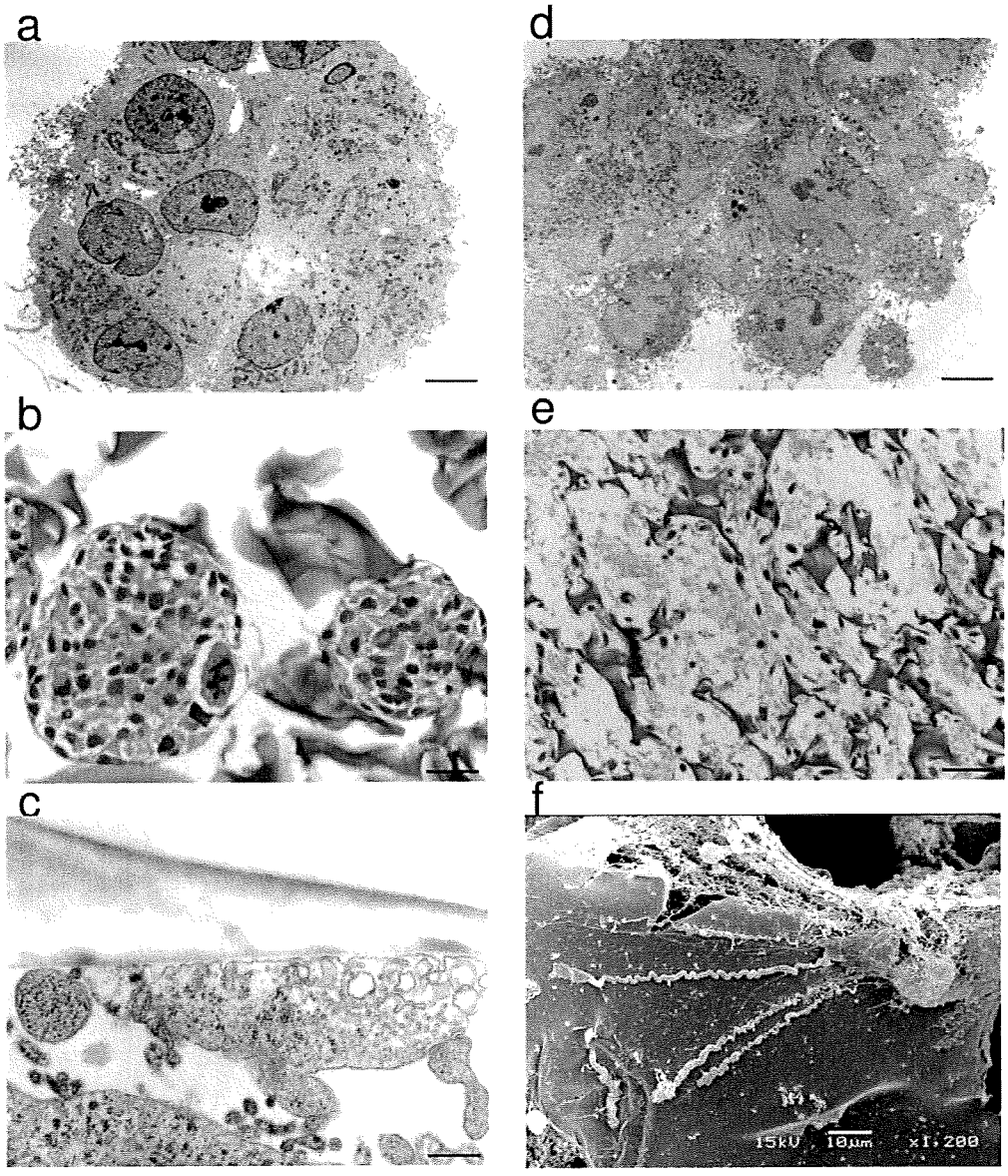

Figure 3. *Morphology of three-dimensionally cultured KNS42, A172 and U118MG cells. a: TEM image of KNS42 cells. Cells aggregated with numerous microvilli in the extracellular spaces as well as on the outside surface of the structure. Bar, 8 μm. b: Cross-section of KNS42 cells forming a spheroid structure (hematoxylin-eosin staining). Note the presence of attachments to the scaffold. Magnification, ×40; bar, 40 μm. c: TEM image of a KNS42 cell attached to the scaffold with distinct extracellular matrix. Bar, 500 nm. d: TEM image of A172 cells with a ragged and lumpy surface and prominent microvilli. Bar, 8 μm. e: Cross-section of U118MG cells (H-E staining) demonstrating an infiltrative pattern and abundant extracellular fibers. Magnification, ×10; bar, 160 μm. f: SEM image of U118MG cells firmly attached to the scaffold by fibers and long processes projecting from the cell body. Microvilli occurred on the tips of the processes.*

extended from the cells and attached to the scaffold with further extension of small fibers that also attached to the scaffold (Figure 3f). Many microvilli were seen on the tips of the processes. These features were unique to U118MG. Cellular connection was usually achieved *via* the cell processes.

Discussion

Malignant glioma is one of the intractable diseases of the human body. In spite of recent advances in medical technologies, malignant glioma is refractory to most current therapies and alternative therapies are required. One

advantage for the development of an effective treatment is that malignant glioma cells seldom metastasize to organs other than the central nervous system and long-term survival or even a cure of the disease could be expected by inhibiting local tumor recurrence. Therefore numerous studies have been carried out using glioma cells. Under such circumstances, the development of an experimental model that simulates an intracranial glioma is important (26, 27), because most studies have been performed on cultures with ordinary monolayer cells.

In a recent study, we optimized therapeutic ultrasound against malignant brain tumor, especially glioma, using a three-dimensional cell culture (28). The data obtained were directly applicable to *in vivo* animal studies and we noted the importance of the nature of the culture. In the present study, the tendency of T98G cells to enter a viable G_1-arrested state when crowded (22) was confirmed in an ordinary two-dimensional cell culture (data not shown). In contrast, glioma cells in three-dimensional culture kept on proliferating at least until day 20 under the current experimental conditions. The difference might be attributable to the abundant scaffold spaces of the three-dimension cell culture. The morphology observed in three-dimensional culture was quite different from that of cells in a conventional monolayer culture. Each glioma has different properties for growth and infiltration into brain parenchyma *in vivo* and these abilities may influence the prognosis of host patients. When the different glioma cells were grown in the scaffold, they displayed notably different characteristics. The U118MG cells dispersed, while the KNS42 and A172 cells conglomerated. After the cells were inoculated on to the scaffold, only those that were attached to the scaffold started to divide, and these cells proliferated *ad locum*. Whether the cells dispersed or conglomerated could have been attributable to different migratory or locomotive abilities. While the U118MG cells tended to separate, the KNS42 and A172 cells did not migrate even after division.

The cells used in this study were representative of standard glioma lines widely used experimentally, both *in vitro* and *in vivo*. These cells were much alike in two-dimensional cell culture. However, different characteristics became evident only after three-dimensional cell culture. It is concluded that culture experiments should be planned with consideration to the individuality of each tumor cell type. There may be many different types of three-dimensional culture methods (29-33) other than the one presented here, suitable for the evaluation of expansion or invasion of glioma. While the morphology of the gliomas was demonstrated using the present scaffold method, a better system that replicates the intra-cerebral environment for malignant cells is required. This may also apply to cells other than gliomas. Accordingly, further study is warranted.

References

1 Pampaloni F, Reynaud EG and Stelzer EH: The third dimension bridges the gap between cell culture and live tissue. Nat Rev Mol Cell Biol *8*: 839-845, 2007.

2 Kleinman HK, Philp D and Hoffman MP: Role of the extracellular matrix in morphogenesis. Curr Opin Biotechnol *14*: 526-532, 2003.

3 Pilkington GJ, Bjerkvig R, De Ridder L and Kaaijk P: *In vitro* and *in vivo* models for the study of brain tumour invasion. Anticancer Res *17*: 4107-4109, 1997.

4 Kleinman HK and Jacob K: Invasion assays. Curr Protoc Cell Biol Chapter *12*: Unit 12-2, 2001.

5 Kleinman HK and Martin GR: Matrigel: basement membrane matrix with biological activity. Semin Cancer Biol *15*: 378-386, 2005.

6 Marques MM, Martins MD and Franca CM: Effect of Matrigel on adenoid cystic carcinoma cell line differentiation. Int J Exp Pathol *87*: 405-410, 2006.

7 de Ridder L, Cornelissen M and de Ridder D: Autologous spheroid culture: a screening tool for human brain tumour invasion. Crit Rev Oncol Hematol *36*: 107-122, 2000.

8 Kunz-Schughart LA, Kreutz M and Knuechel R: Multicellular spheroids: a three-dimensional *in vitro* culture system to study tumour biology. Int J Exp Pathol *79*: 1-23, 1998.

9 Mizuno S and Glowacki J: Three-dimensional composite of demineralized bone powder and collagen for *in vitro* analysis of chondroinduction of human dermal fibroblasts. Biomaterials *17*: 1819-1825, 1996.

10 Mizuno S and Glowacki J: Chondroinduction of human dermal fibroblasts by demineralized bone in three-dimensional culture. Exp Cell Res *227*: 89-97, 1996.

11 Allemann F, Mizuno S, Eid K, Yates KE, Zaleske D and Glowacki J: Effects of hyaluronan on engineered articular cartilage extracellular matrix gene expression in 3-dimensional collagen scaffolds. J Biomed Mater Res *55*: 13-19, 2001.

12 Yates KE, Mizuno S and Glowacki J: Early shifts in gene expression during chondroinduction of human dermal fibroblasts. Exp Cell Res *265*: 203-211, 2001.

13 Glowacki J and Mizuno S: Collagen scaffolds for tissue engineering. Biopolymers *89*: 338-344, 2008.

14 Mizuno S and Glowacki J: Low oxygen tension enhances chondroinduction by demineralized bone matrix in human dermal fibroblasts *in vitro*. Cells Tissues Organs *180*: 151-158, 2005.

15 Mueller SM, Mizuno S, Gerstenfeld LC and Glowacki J: Medium perfusion enhances osteogenesis by murine osteosarcoma cells in three-dimensional collagen sponges. J Bone Miner Res *14*: 2118-2126, 1999.

16 Navarro FA, Mizuno S, Huertas JC, Glowacki J and Orgill DP: Perfusion of medium improves growth of human oral neomucosal tissue constructs. Wound Repair Regen *9*: 507-512, 2001.

17 Glowacki J, Mizuno S and Greenberger JS: Perfusion enhances functions of bone marrow stromal cells in three-dimensional culture. Cell Transplant *7*: 319-326, 1998.

18 Mizuno S, Allemann F and Glowacki J: Effects of medium perfusion on matrix production by bovine chondrocytes in three-dimensional collagen sponges. J Biomed Mater Res *56*: 368-375, 2001.

19 Mizuno S, Tateishi T, Ushida T and Glowacki J: Hydrostatic fluid pressure enhances matrix synthesis and accumulation by bovine chondrocytes in three-dimensional culture. J Cell Physiol *193*: 319-327, 2002.
20 Mizuno S: A novel method for assessing effects of hydrostatic fluid pressure on intracellular calcium: a study with bovine articular chondrocytes. Am J Physiol Cell Physiol *288*: C329-337, 2005.
21 Manome Y, Saeki N, Yoshinaga H, Watanabe M and Mizuno S: A culture device demonstrates that hydrostatic pressure increases mRNA of RGS5 in neuroblastoma and CHC1-L in lymphocytic cells. Cells Tissues Organs *174*: 155-161, 2003.
22 Stein GH: T98G: an anchorage-independent human tumor cell line that exhibits stationary phase G_1 arrest *in vitro*. J Cell Physiol *99*: 43-54, 1979.
23 Giard DJ, Aaronson SA, Todaro GJ, Arnstein P, Kersey JH, Dosik H and Parks WP: *In vitro* cultivation of human tumors: establishment of cell lines derived from a series of solid tumors. J Natl Cancer Inst *51*: 1417-1423, 1973.
24 Ponten J and Macintyre EH: Long term culture of normal and neoplastic human glia. Acta Pathol Microbiol Scand *74*: 465-486, 1968.
25 Takeshita I, Takaki T, Kuramitsu M, Nagasaka S, Machi T, Ogawa H, Egami H, Mannoji H, Fukui M and Kitamura K: Characteristics of an established human glioma cell line, KNS-42. Neurol Med Chir *27*: 581-587, 1987.
26 Corcoran A, De Ridder LI, Del Duca D, Kalala OJ, Lah T, Pilkington GJ and Del Maestro RF: Evolution of the brain tumour spheroid model: transcending current model limitations. Acta Neurochir *145*: 819-824, 2003.
27 Grobben B, De Deyn PP and Slegers H: Rat C6 glioma as experimental model system for the study of glioblastoma growth and invasion. Cell Tissue Res *310*: 257-270, 2002.
28 Manome Y, Furuhata H, Hashimoto A, Funamizu N, Suzuki R, Ishizawa S, Akiyama N, Kobayashi T and Watanabe M: Application of therapeutic insonation to malignant glioma cells and facilitation by echo-contrast microbubbles of levovist. Anticancer Res *29*: 235-242, 2009.
29 Friedl P and Wolf K: Tumour-cell invasion and migration: diversity and escape mechanisms. Nat Rev Cancer *3*: 362-374, 2003.
30 Hegedüs B, Marga F, Jakab K, Sharpe-Timms KL and Forgacs G: The interplay of cell-cell and cell-matrix interactions in the invasive properties of brain tumors. Biophys J *91*: 2708-2716, 2006.
31 Kaufman LJ, Brangwynne CP, Kasza KE, Filippidi E, Gordon VD, Deisboeck TS and Weitz DA: Glioma expansion in collagen I matrices: analyzing collagen concentration-dependent growth and motility patterns. Biophys J *89*: 635-650, 2005.
32 Stein AM, Demuth T, Mobley D, Berens M and Sander LM: A mathematical model of glioblastoma tumor spheroid invasion in a three-dimensional *in vitro* experiment. Biophys J *92*: 356–365, 2007.
33 Werbowetski T, Bjerkvig R and Del Maestro RF: Evidence for a secreted chemorepellent that directs glioma cell invasion. J Neurobiol *60*: 71-88, 2004.

Received August 25, 2009
Revised January 19, 2010
Accepted January 21, 2010

Biochemical and Biophysical Research Communications 381 (2009) 612–618

Contents lists available at ScienceDirect

Biochemical and Biophysical Research Communications

journal homepage: www.elsevier.com/locate/ybbrc

Enhancing activity of *N*-glycosylation for constitutive proteins secretions in non-polarized cells

Nobutake Akiyama [a,*], Yuji Ohno [b], Takahiro Fukuda [c], Yosinobu Manome [d], Saburo Saito [a]

[a] Department of Molecular Immunology, Institute of DNA medicine, Jikei University, 3-25-8 Nishi-Shinbashi, Minato-ku, Tokyo 105-8461, Japan
[b] Department of Pharmacology, Jikei University School of Medicine, 3-25-8, Nishi-Shinbashi, Minato-ku, Tokyo 105-8461, Japan
[c] Division of Neuropathology, Dept. of Neuroscience, Research Center of Medical Science, The Jikei Univ. Schl. Med., 3-25-8 Nishi-Shimbashi, Minato-ku, Tokyo 105-8461, Japan
[d] Department of Molecular Cell Biology, Institute of DNA medicine, Jikei University, 3-25-8 Nishi-Shinbashi, Minato-ku, Tokyo 105-8461, Japan

ARTICLE INFO

Article history:
Received 8 February 2009
Available online 25 February 2009

Keywords:
N-Glycosylation
Constitutive protein secretion
Interleukin-31

ABSTRACT

Several fusion proteins of mouse Interleukins (mILs) and the enhanced green fluorescent protein (EGFP) were expressed in fibroblast and epithelial cells. Among these proteins, the mIL-31 derivative was the most efficiently secreted into the medium in a *N*-glycosylation-dependent manner. From the analysis of deletion mutants, the minimal structure for constitutive secretions consisted of a signal peptide and *N*-glycosylation. Introduction of the signal sequence from mIL-31 to human p53 protein failed to secrete the products, but further addition of the *N*-glycosylation site resulted in constitutive secretion of biologically active p53 protein into the medium in the *N*-glycosylated form. In this report, we showed the importance of *N*-glycosylation for constitutive protein secretions, especially using non-polarized cells.

Introduction

Signal transduction proteins perform their function after transportation to the plasma membrane or extracellular secretion, and such proteins are usually glycosylated. The influence of glycosylation on protein trafficking has been studied mainly with polarized cells. Two pathways for the secretion of proteins have been reported [1]: one is a conventional pathway and the other is an unconventional pathway [2]. Most of the secretory proteins utilize the conventional pathway, and they follow a route to the plasma membrane via the endoplasmic reticulum (ER) and Golgi apparatus. These proteins have signal peptides that are trapped and sent into the ER by the signal recognition particle [3].

The proteins are further modified, for example by *N*/*O*-glycosylation and glycosyl-phosphatidyl-inositol anchoring in the ER and Golgi apparatus. Protein modifications have an influence on the sorting of secretion vesicles containing proteins, which head apical or basolateral sides. These mechanisms have been studied intensively with polarized cell lines [4–6].

The mechanism of constitutive protein secretion in non-polarized cells has been paid little attention [7], with several reports describing the discovery of the secretory mechanism without considering *N*/*O*-glycosylation and other protein modifications [8], but these studies were conducted with substantially secretable proteins.

In our preliminary study, we observed excellent secretory properties of mouse Interleukin 31 (mIL-31) when this cDNA was expressed in epithelial and fibroblast cells. Mouse IL-31 is a four-helix bundle containing Th2 cytokine flanking 4 asparagine-linked *N*-glycosylation sites and this cytokine is assumed to be a substantial mediator of the itch sensation with atopic dermatitis [9–11].

To identify the underlying cause of these secretions, we analyzed the secretion properties of mIL-31 protein.

Materials and methods

Preparation of anti-mouse IL-31 polyclonal antibody. cDNA spanning amino acid 24–163 of mIL-31 was cloned in frame with pET30A (Novagen) and the construct was transformed in BL-21 cells (Novagen). After induction with isopropyl-β-D-thiogalactopyranoside (IPTG), mIL-31 protein was purified under denaturation conditions by nickel-chelating sepharose (Qiagen), dialyzed in PBS, and used as immunogen (mIL-31 protein). Two male rabbits (Japanese White rabbit) were immunized with mIL-31 proteins using the complete Freund adjuvant, boosted with incomplete Freund adjuvant twice at an interval of 2 weeks and blood was

Abbreviations: ER, endoplasmic reticulum; IL, interleukin; PCR, polymerase chain reaction; ATP, Adenosine tri-phosphate; PAGE, polyacrylamide gel electrophoresis; PVDF, polyvinylidene difluoride; EGFP, enhanced green fluorescent protein; GPI, glycophosphatidylinositol; IPTG, isopropyl-β-D-thiogalactopyranoside; CFA, complete Freund adjuvant; IFA, incomplete Freund adjuvant.

* Corresponding author. Fax: +81 3 3435 1922.
E-mail address: nakiyama@jikei.ac.jp (N. Akiyama).

0006-291X/$ - see front matter © 2009 Elsevier Inc. All rights reserved.
doi:10.1016/j.bbrc.2009.02.101

collected under anesthesia. The antibody was purified from the serum with immobilized mIL-31 protein sepharose.

Plasmid constructions. Full length cDNAs (mIL-4 (GeneBank Accession No. NM_021283), mIL-5 (GeneBank Accession No. NM_010558), mIL-6 (GeneBank Accession No. NM_031168), mIL-12 (GeneBank Accession No. NM_008351), mIL-13 (GeneBank Accession No. NM_008355), mIL-31 (GeneBank Accession No. AY509149), mIL-33 (GeneBank Accession No. NM_133775)) flanking restriction sites were amplified from spleen cDNA of Balb/C and human p53 cDNA (GeneBank Accession No. NM_000546) were amplified from human peripheral blood monocytic cells cDNA by PCR, and subcloned into pBluescript 2SK+ (Stratagene). The coding region of fluorescent protein was amplified from pEGFP-C1 (Clonetech) vector or pDsRed-Monomer-C1 (Clonetech) by PCR and subcloned into pBluescript2 SK+. With this insert, the desired cDNA was generated, and subcloned into pcDNA3.1-MH-A+ (Invitrogen) with the CMV promotor. The structures of the expression cassettes are summarized in Figs. 1C, 2A, and 3A. The detailed constructions are described in supplementary data #1.

Protein expression. HEK-293 cells were maintained in Dulbecco's modified Eagle's medium (Invitrogen, Carlsbad, CA, USA) with 10% fetal bovine serum (Hyclone, Logan, UT, USA) or Low immunoglobulin fetal bovine serum (Invitrogen) and antibiotics (Invitrogen). Expression plasmids were transfected to HEK-293 cells and COS-1 cells by Lipofectamine2000 (Invitrogen) according to the manufacturer's instructions.

Maintenance and transfection of FreeStyle 293 cells (Invitrogen) were processed as described by the manufacturer.

Western blot analysis. After cells were spun down at 800 *g* for 10 min, we collected the supernatant and suspended the cell pellets in PBS. Cell pellets and supernatants were treated with Laemmli's sample buffer and boiled for 5 min [12]. The samples were run on SDS–PAGE gels [13], semi-dry blotted on PVDF membranes (Sequi-Blot PVDF membrane, Bio-Rad Lab., CA, USA), and the membranes were processed with the Can-Get-Signal Western blot detection kit (TOYOBO Co. Ltd., Osaka, Japan) using anti-His Tag (MBL Co. Ltd., Nagoya, Japan) or anti IL-31 antibody and appropriate HRP-conjugated 2nd antibody, according to the manufacturer's instructions. They were visualized by chemiluminescence (Amersham ECL Plus, Uppsala, Sweden) followed by exposure to Hyperfilm-ECL.

Purification of secreted proteins. Secreted recombinant proteins flanking the histidine tag were prepared as follows: the supernatants were collected after centrifugation at 1000 r.p.m for 15 min, and the solutions adjusted to 0.5 M NaCl, 50 mM Tris–Cl (pH 7.4), and 10 mM imidazole. Histidine-tagged proteins were captured on an Ni–NTA–agarose column equilibrated with an equilibration buffer (to 0.5 M NaCl, 50 mM Tris–HCl (pH 7.4), 10 mM

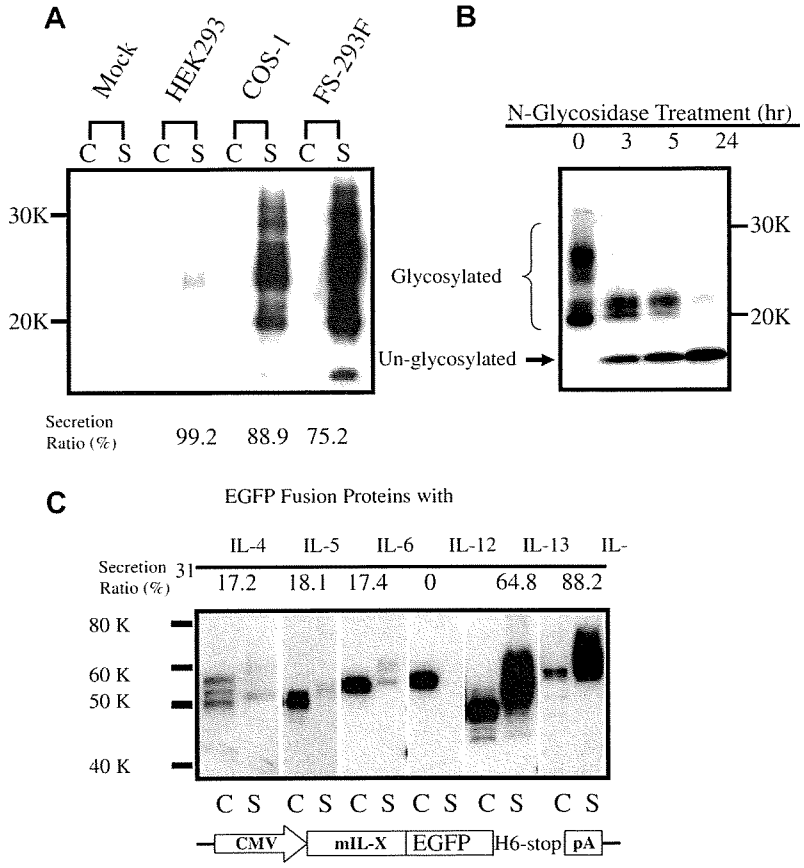

Fig. 1. Expression and secretion of interleukins derivatives. (A) IL-31 secretion in the three cell lines. HEK 293 cells and COS-1 cells (adhesive cell lines) were harvested on day 2 and FreeStyle 293F cells were harvested as described under "Materials and methods". IL-31 was detected by Western blot/ECL Plus reaction with rabbit anti-IL-31 with Can Get Signal® Immunoreaction Enhancer Solution. C, cell; S, supernatant. Secretion efficiencies (secreted amount of mIL-31/total expressed amount of mIL-31) were determined and are listed with the densitometry analysis of each lane in Figure 1 by "Quantity One" (Bio Rad Inc.) densitometry analyzing software. (B) Deglycosylation of secreted IL-31. IL-31 in the supernatant was denatured and digested with *N*-glycosidase-F for the indicated time. (C) Secretion of EGFP-fusion Proteins with Interleukins from FS 293F Cells. Transfected FreeStyle 293F cells were harvested and cellular material and supernatant were analyzed by Western blot/ECL Plus reaction by detecting the histidine tag at the C terminal end. The secretion efficiencies were determined by densitometry analysis performed as panel A.

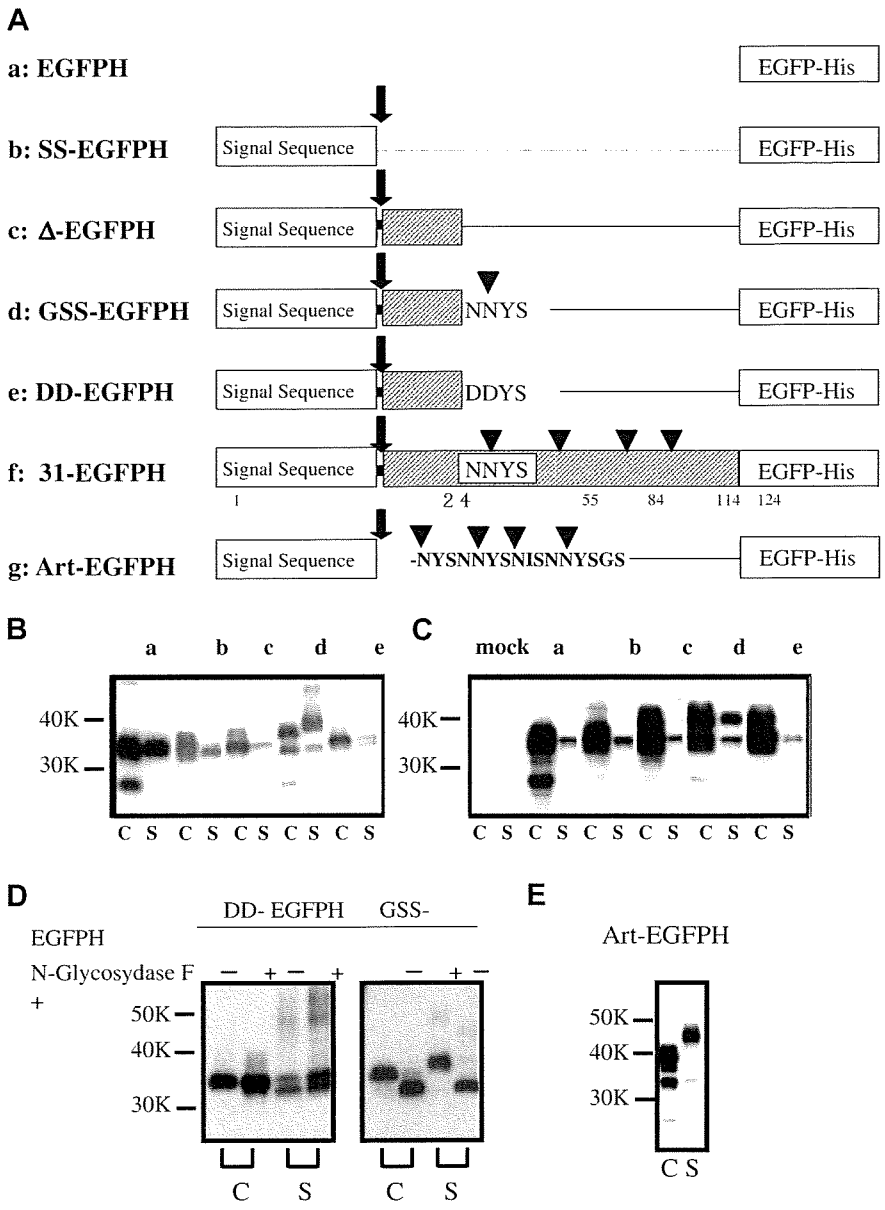

Fig. 2. Glycosylation promotes the expressed proteins. (A) Schematic amino acid sequences of various EGFPH-fusion proteins with IL-31 derivatives. Signal sequence indicates the first 23 amino acids of the N-terminal of IL-31. The arrows and arrow heads denote the cleavage site and putative glycosylation sites, respectively. The hatched boxes and numbers under the boxes designate amino acids derived from IL-31 and the number of the amino acid indicates the position of the putative *N*-glycosylation sites of IL-31. His, 6× His (His Tag). (B,C) Immunoblot analysis of cellular and supernatant fractions in (B) expressed in FreeStyle 293 cells and (C) in Cos-1 cells. The expressed proteins were detected by histidine tags at the C-terminal end. C, cell; S, supernatant. (D) Deglycosylation of GSS(DD)-EGFPH and GSS-EGFPH. Denatured GSS(DD)-EGFPH and GSS-EGFPH in the cell and in the supernatant were digested with *N*-glycosidase-F for 7 h under denatured conditions. (E) Secretion of Art-EGFPH protein. Four artificially designed consecutive glycosylation sites were located after the signal sequence. The fusion proteins were expressed in FreeStyle 293 cells and histidine tags were detected with Western blot analysis.

imidazole), washed in 3 bed volumes of equilibration buffer and eluted with equilibration buffer containing 0.25 M imidazole; the elution was dialyzed in PBS.

Removal of glycosylation. *N*-Glycosidase digestion—In the denatured condition, aliquots of supernatant or cell lysate were boiled for 5 min in a buffer containing 50 mM sodium phosphate buffer (pH 7.5), 0.1% SDS and 50 mM β-mercaptoethanol. Next, the denatured samples were cooled and incubated at 37 °C for the appropriate time after the addition of 0.75% Triton X-100 and 0.5 mU *N*-glycosidase-F.

Binding assay to p53 consensus sequence. The culture supernatants were obtained by centrifugation. We evaluated the binding activities to a p53 consensus binding site (5̂-GGACATGCC CGGGCATGTCC-3̂) by Trans AM (Active motif: CA, USA) in accordance with the manufacturer's recommendation.

Results

Efficient secretion properties of mIL-31 and derivatives

To confirm the high secretory efficiency of mIL-31 in different cell lines, we transfected the expression vector of mIL-31 into COS-1 (Transformed African monkey kidney fibroblast), HEK-293 (Human embryo kidney epithelial cell) and FreeStyle 293F cells

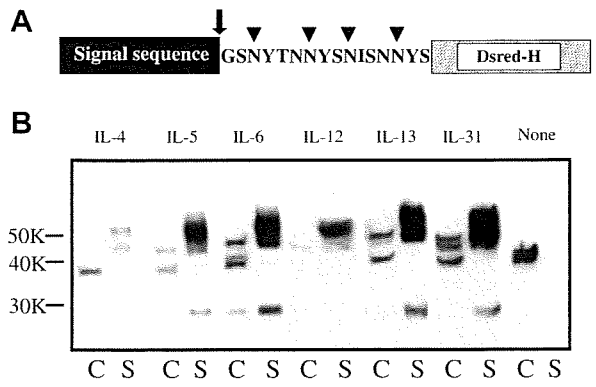

Fig. 3. The glycosylations mainly influenced constitutive proteins secretion, not the structure of the signal sequences. (A) The structure of Dsred derivatives. Solid and hatched boxes indicate the signal sequence of mouse Interleukin and Dsred proteins flanking the histidine tag, respectively. Arrow and arrow heads indicate the cleavage site of signal peptidase and the putative *N*-glycosylation sites, respectively. Putatively, the primary structures of the cleaved products were equal in spite of the different sequence of signal peptides after cleavage by signal peptidase. (B) The secretion efficiencies were independent of the sequence of signal peptides. Dsred derivatives were expressed in FreeStyle 293-F cells. The cellular fraction (C) and the supernatant (S) were detected by histidine tags with Western blot analysis.

(FS293F: a variant of HEK-293; Invitrogen inc.), and measured the secretion efficiency by Western blot analysis (Fig. 1A). The molecular weight of mature mIL-31 protein was predicted to be about 15,600 after cleavage at Ala23 by a signal peptidase. Faint bands matched the calculated molecular weight, but the major bands were higher than predicted, ranging between 19 and 30 kDa in all cell lines. The increased molecular weight was considered to be the result of modification by *N*-glycosylation. Densitometry analysis confirmed that more than 75% of the produced proteins were released into the medium with all cell lines (Fig. 1B).

This cytokine contains four putative *N*-glycosylation sites containing the NX(S/T) motif [14] at positions 55, 84, 114, and 124, and the broad distribution of molecular weight possibly indicates the multiple *N*-glycosylation of asparagine residues with different carbohydrates. This massive increase in molecular weight resulting from *N*-glycosylation is a distinct characteristic of the mIL-31 protein. To determine whether the mIL-31 protein expressed in FS-293F cells is an *N*-glycosylated protein or not, the secreted proteins were treated with *N*-glycopeptidase-F, which cleaves the linkages between the innermost GlcNAc and asparagine residues of N-linked glycoproteins (Fig. 1B) [15]. After treatment with this enzyme, the broad band almost converged on the lowest band whose molecular weight matched the mIL-31-predicted size computationally. This result confirmed that the major cause of the increase in molecular weight was modification by *N*-glycosylation and not by *O*-glycosylation.

Comparison of secretion efficiency between several cytokines

Since mIL-31 was secreted efficiently, we compared the secretion efficiencies between Interleukin-4/5/6/12(p35)/13/31 when the proteins were expressed as an EGFP fusion protein.

It has been already reported that IL-1β is secreted after cleavage by Caspase-1 [2], hence this type of cytokine was omitted from the investigation.

Western blot images and their densitometry analyses using detection with the histidine tag at the C-terminal end revealed that EGFPH-fusion proteins with m-IL4, 5, and 6 were secreted poorly (<20%), but m-IL13-EGFPH (65%) and m-IL-31-EGFPH (86%) proteins were secreted effectively (Fig. 1C). Interestingly, the molecular weights of the secreted proteins were different from those of the non-secreted proteins in all lanes, thereby suggesting that the difference in protein modification was reflected in their secretion properties. The major candidate for this protein modification was *N*-glycosylation since the cDNA contained the consensus sequence of *N*-glycosylation.

There are three possible *N*-glycosylation sites in IL-4, 5, and 13 according to a computer prediction from the primary structure: IL-6 has no putative *N*-glycosylation sites and IL-12 has only one site. The secretion efficiency did not seem to be correlated to the number of sites, but the actual status of glycosylation cannot be easily predicted.

The IL-6-EGFPH protein did not contain a possible *N*-glycosylation site as this cytokine was probably *O*-glycosylated. Since there are 20 asparagine residues in IL-6 amino acids, the possibility of *N*-glycosylation could not be omitted.

Among these cytokines, mIL-31 showed the strongest secretion property, hence further analysis was focused on the structure of mIL-31, particularly on the effect of *N*-glycosylation of secretory proteins.

Necessity of N-glycosylation for the secretion of mIL-31 and EGFP chimera

Several groups have reported that the *N*-glycosylation modification is essential for the secretion of some proteins [16] since removal of the *N*-glycosylation sites by site-directed mutation [17] reduced the secretion. Furthermore the additions of *N*-glycosylation resulted in apical secretion [18,6], but whether or not *N*-glycosylation is sufficient in the presence of signal sequences, especially in the case of manufactured proteins, remains unclear.

We constructed several mutants of mIL-31 and EGFP fusion cDNA with attention to the *N*-glycosylation modifications. The structures of these mutants are summarized in Fig. 2A. cDNA was expressed in FreeStyle 293F cells and secretion of the expressed product was analyzed with Western blot analysis (Fig. 2B). We had postulated that the EGFPH itself remains in the cells, but EGFPH protein was present in the medium. The expression level of EGFPH was considerably higher than that of other proteins. One possible explanation is cytotoxicity of EGFP in cases of overexpression [19], causing the cells to burst, releasing their components. However, GSS-EGFPH was secreted the most efficiently into the medium. The possible *N*-glycosylation site with the NX(S/T) motif lies only at position 55–57 and the absence of *N*-glycosylation by deletion or mutation was correlated to a low level of protein secretion (lanes b–e). The same tendencies were observed with COS-1 fibroblast cells, even though the secretion rates were lower than for FS-293F cells (Fig. 2C).

To investigate the influence of the *N*-glycosylation on protein secretion, secreted or non-secreted proteins were treated with *N*-glycopeptidase-F with DD or GSS-EGFPH proteins. In the case of DD-EGFPH, which does not contain any *N*-glycosylation sites, there were no differences in molecular weight caused by the cleavage of sugar moieties, but the products in the supernatant fraction were doublet bands, which might have derived from other types of protein modification. In the case of the GSS-EGFPH protein, digestion indicated that both the intra- and extra-cellular proteins were *N*-glycosylated, but the molecular weight of undigested, non-secreted protein was higher than that of non-secreted DD-EGFPH. The molecular weights of the secreted proteins were higher than those of the non-secreted proteins in the case of GSS-EGFPH. This indicated that both the secreted and non-secreted proteins were *N*-glycosylated, but *N*-glycosylation alone was not sufficient for protein secretion. It also indicated that there are some structural differences in *N*-glycosylation that regulate protein secretions (Fig. 2D).

To demonstrate that *N*-glycosylation was important and not the proteinaceous structure between the cleavage and glycosylation sites, we designed an EGFPH derivative with a signal sequence and four consecutive artificially designed glycosylation sites (Art-EGFPH).

The design is shown in Fig. 2A–g. As predicted, the increases in molecular weights were observed as a result of *N*-glycosylation, and constitutive secretion was enhanced as in the GSS-EGFPH protein (Fig. 2E).

The comparison of signal peptides from several cytokines

In Fig. 3, a different kind of signal sequence was fused to red fluorescent protein (Dsred-H) with artificially designed *N*-glycosylation sites, and expressed in FreeStyle 293-F cells. The structure is summarized in Fig. 3A. The Dsred-H protein is a monomeric fluorescent protein that is less cytotoxic than the EGFP protein. After cleavage by a signal peptidase, the primary structure of the expressed products was the same, hence in this experiment the "strength" of the signal peptide was measurable. Unlike EGFP derivatives, the Dsred derivative without a signal peptide remained in the cells, but the addition of any kind of signal peptide led to the efficient secretion of products. Accordingly, from the viewpoint of protein secretion efficiency, the influence of the different signal peptide could not be observed (Fig. 4B).

Application to functional mammalian proteins

Since the minimal region (GSS) was identified for protein secretion, we constructed the fusion protein with human p53 and IL-33 protein. Three kinds of p53 derivative were expressed (p53H, SS-p53H, and GSS-p53H proteins) in FS 293F cells (Fig. 4A). Only the GSS-p53H protein was secreted as an *N*-glycosylated form, but p53H and SS-p53H were not secreted into the supernatants. The secretory rate of GSS-p53H was 26% as determined by densitometry analysis of Western blots. Since the p53 protein contains four possible *N*-glycosylation motifs, the modification might have occurred in the region of the p53 protein, but as the SS-p53 protein was not secreted, the region in GSS might have been *N*-glycosylated.

Next, we examined the binding activities of the culture medium to p53 recognition consensus sequences [20]. In a mock vector, no trace activity was detected in the medium (data not shown), and addition of the signal sequence and glycosylation sequence (GSS-p53H) resulted in a significant amount of binding activity in the medium. The trace activity was observed in the medium in the case of p53H, and this phenomenon can be explained by the result of cells bursting as with the case of EGFP-H (Fig. 4B).

Purification of GSS-p53H from the medium with nickel-chelating sepharose enriched the binding activity 140-fold, and 30% of the binding activity was restored by simple column purification (Fig. 4C). It is important to note that purification was performed without the use of strong detergents and chaotropic reagents that usually have an influence on the activities of the products.

Mouse IL-33 is a chemokine that regulates IgE expression, and its secretion [21] is thought to require cleavage by a protease (possibly Caspase-1), [22]. Mouse IL-33H with a naïve signal sequence and a flanking histidine tag was not secreted, but the chimera with an IL-31-derived signal peptide and core region of mIL-33 with this tag was constitutively secreted with an increase in the calculated molecular weight. (Fig. 4D) In this case, the mature cytokine was secreted without an additional *N*-glycosylation site, because the mature mIL-33 has a putative glycosylation site at the asparagine residue located at the 182nd amino acid from the N-terminus of the immature mIL33 protein.

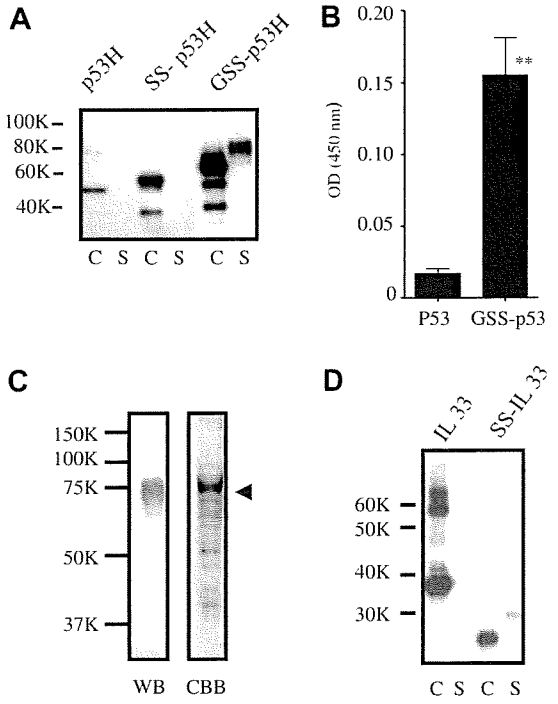

Fig. 4. The IL-31 Fusion Protein with Functional Mammalian Proteins. (A) Secretion of p53-fusion proteins with N-terminal amino acids of IL-31. The prefixes of p53 have the same meanings as in Fig. 2A and suffix of H as His Tag. (B) The DNA binding ability of GSS-p53H to the p53 consensus sequences. The DNA binding activity of the culture medium was estimated by TransAM™ p53 (Active Motif). Results are reported as means ± SE from five independent samples for each transfection. $^{**}P < 0.01$, compared with the p53H supernatant with the Student's *t*-test. (C) SDS-PAGE analysis of GSS-p53H. Western blotting analysis of the culture supernatant was performed using anti-His-tag antibody. Secreted GSS-p53H was concentrated with a Ni-column and Amicon Ultra-15 (10,000 MWCO). The concentrated GSS-p53H was stained by Coomassie brilliant blue. The secreted GSS-p53H is indicated by the arrowhead. (D) The exchange of the signal sequence from IL-33 to IL-31 enhanced the secretion of IL-33 proteins. C, cell; S, supernatant.

Discussion

There have been numerous analyses conducted on the mechanisms of secretion in polarized cells, especially in Madin–Darby canine kidney (MDCK) cells [5,4]. The trafficking or sorting of proteins has been exhaustively investigated, especially in polarized cells and several components related to sorting signals and adaptor proteins have been identified. The secreted proteins take two pathways [23,2]: one is a conventional pathway and the other is unconventional. Fibroblast growth factor-2 (FGF-2), interleukin 1β [24], and Leishmania hydrophilic acylated surface protein B (HASPB) take the latter pathway for secretion [23]. On the contrary, most of the proteins are exported from mammalian cells via the former pathway.

Furthermore, both pathways possess two secretory pathways, respectively [25,1]. One is a constitutive pathway for immediate secretion and the other is a regulated pathway for accumulation and secretion under stimulation. However, some cytokines might adapt these manners for secretion. IL-10 takes the constitutive pathway for basal secretion, whereas it takes the regulated pathway for secretory stimulation. However, among cytokines, IL-10 [26,27] and IL-6 [28] have reported to take the constitutive secretion pathway, and there have been few reports of cytokines that were secreted like mIL-31. Even albumin, which is a representative of constitutive secretion, could not be effectively released like this cytokine [29].

We predicted that fusion proteins with mIL-31 could have enhanced secretion. In MDCK cells, it was reported that *O*-glycosylation of the neurotrophin receptor [5] and *N*-glycosylation of erythropoietin [4] were related to their secretion, hence it has been reported that glycosylation is one of the critical factors underlying apical secretion in polarized cells. The mechanisms were investigated mainly with polarized cell lines, and the apical targeting was critical for protein secretion. In a non-polarized cell line, such sorting is irrelevant, because a cell does not have polarity.

In our study, we showed that IL-31 (1–57) from the signal peptide to the first *N*-glycosylation sequences (GSS) was effective for secretion of the EGFP-fusion protein, and that *N*-glycosylation is an enhancer of secretion of proteins with this signal peptide in a non-polarized cell line (e.g., fibroblasts and epithelial cells). *N*-Glycans should be modified to a mature secretory protein in the late ER or Golgi apparatus. The glycosylated protein remaining in the cells must be stacked on the ER and Golgi apparatus or they would be an intermediate form to the secretory ones. Further modifications of oligosaccharides like sialylation have been reported to play a critical role in the control of the secretion in MDCK cells [30].

There are several contradicting reports about the importance of *N*-glycosylation for protein localization to the plasma membranes or out of the membranes. For example, in the case of CD4 proteins, the Tifft group reported that localization of the CD4 protein on the cell membrane was blocked by the treatment of tunicamycin or removal of the glycosylation site [31] as in our study. In another case, soluble secretory CD4 protein that lacks a plasma membrane anchoring sequence was secreted even when the *N*-glycosylation site was removed.

There are other structures implicated in the apical sorting (*O*-glycan, GPI anchoring signal, proteinaceous sequences in hemagglutinin of the influenza virus, cytoplasmic domain of rhodopsin), which are concerned with protein secretion.

In the case of non-polarized cell lines, our data suggested that *N*-glycosylation enhanced constitutive secretion, but not all of the *N*-glycosylation products were secreted in the case of GSS-EGFPH. Significant amounts of *N*-glycosylated products remained in the cell fraction, suggesting that some mature structure of *N*-glycosylation is required for constitutive secretion. Details of the glycosylation form that controls constitutive secretion should be further analyzed.

Fig. 3 confirms the importance of *N*-glycosylation for protein secretion, but the advantage of the signal peptide of mIL-31 was not observed. However, Fig. 4D shows that the signal peptide of mIL-31 was more effective than the original signal peptide of mIL-33. The signal peptide that targets the ER could be chosen for constitutive protein secretion in combination with *N*-glycosylation.

We have demonstrated the usefulness of the signal peptide and *N*-glycosylation for protein preparation using the human p53 protein as a model (Fig. 4). In this experiment, we succeeded in secreting nuclear proteins with the GSS sequence, and not with the signal peptide only. Unlike the EGFP protein, an artificially constructed *N*-glycosylation sequence did not function. With several model proteins, the same tendencies were observed (data not shown). Since the degree of *N*-glycosylation is dependant on the primary structures, we cannot exclude the possibility of the existence of some sequence that accelerates protein secretions with the GSS sequence.

Even the strong secretory property of *N*-glycosylation with the signal sequence of mIL-31 was demonstrated, but there was some limitation: The secreted proteins should not be captured in ER membranes with the hydrophobic stop-transfer sequence that enables integration of the inserting protein released laterally in the ER membrane or membrane-anchoring modifications such as GPI-anchoring modifications.

Once secretion of the proteins is achieved, the secreted proteins can be expected to be more useful than those of other preparations. The proteins were synthesized with mammalian ribosome complex, hence residual activities may have existed because of the correct foldings, and the proteins were free from contaminants, as compared to proteins synthesized by a prokaryote component. As we showed in the preparation of GSS-p53 proteins, proteins are present in a solubilized form at the outset without the use of any detergents. Since the sugar component is very hydrophilic, enhancement of protein solubility can be predicted. Furthermore, it should be noted that these sequences have potential applications for DNA immunization and gene therapy.

Acknowledgments

This work was supported by Grants-in-Aid for Scientific Research from the Ministry of Education and The Jikei University Research Fund. The technical assistance of Ms. Y. Natake is gratefully acknowledged. We thank Prof. Hiroto Okayama for his insightful suggestions.

Appendix A. Supplementary data

Supplementary data associated with this article can be found, in the online version, at doi:10.1016/j.bbrc.2009.02.101.

References

[1] P. Daull, W. Home, D. LeBel, Characterization of the TGN exit routes in AtT20 cells using pancreatic amylase and serum albumin, Eur. J. Cell Biol. 83 (2004) 121–130.
[2] I. Prudovsky, A. Mandinova, R. Soldi, C. Bagala, I. Graziani, M. Landriscina, F. Tarantini, M. Duarte, S. Bellum, H. Doherty, T. Maciag, The non-classical export routes: FGF1 and IL-1alpha point the way, J. Cell Sci. 116 (2003) 4871–4881.
[3] K. Nagai, C. Oubridge, A. Kuglstatter, E. Menichelli, C. Isel, L. Jovine, Structure, function and evolution of the signal recognition particle, EMBO J. 22 (2003) 3479–3485.
[4] Y. Kitagawa, Y. Sano, M. Ueda, K. Higashio, H. Narita, M. Okano, S. Matsumoto, R. Sasaki, *N*-Glycosylation of erythropoietin is critical for apical secretion by Madin–Darby canine kidney cells, Exp. Cell Res. 213 (1994) 449–457.
[5] C. Yeaman, A.H. Le Gall, A.N. Baldwin, L. Monlauzeur, A. Le Bivic, E. Rodriguez-Boulan, The *O*-glycosylated stalk domain is required for apical sorting of neurotrophin receptors in polarized MDCK cells, J. Cell Biol. 139 (1997) 929–940.
[6] J.H. Benting, A.G. Rietveld, K. Simons, *N*-Glycans mediate the apical sorting of a GPI-anchored, raft-associated protein in Madin–Darby canine kidney cells, J. Cell Biol. 146 (1999) 313–320.
[7] T. Yoshimori, P. Keller, M.G. Roth, K. Simons, Different biosynthetic transport routes to the plasma membrane in BHK and CHO cells, J. Cell Biol. 133 (1996) 247–256.
[8] G. Fantuzzi, C.A. Dinarello, Interleukin-18 and interleukin-1 beta: two cytokine substrates for ICE (caspase-1), J. Clin. Immunol. 19 (1999) 1–11.
[9] S.R. Dillon, C. Sprecher, A. Hammond, J. Bilsborough, M. Rosenfeld-Franklin, S.R. Presnell, H.S. Haugen, M. Maurer, B. Harder, J. Johnston, S. Bort, S. Mudri, J.L. Kuijper, T. Bukowski, P. Shea, D.L. Dong, M. Dasovich, F.J. Grant, L. Lockwood, S.D. Levin, C. LeCiel, K. Waggie, H. Day, S. Topouzis, J. Kramer, R. Kuestner, Z. Chen, D. Foster, J. Parrish-Novak, J.A. Gross, Interleukin 31, a cytokine produced by activated T cells, induces dermatitis in mice, Nat. Immunol. 5 (2004) 752–760.
[10] J. Bilsborough, D.Y. Leung, M. Maurer, M. Howell, M. Boguniewicz, L. Yao, H. Storey, C. LeCiel, B. Harder, J.A. Gross, IL-31 is associated with cutaneous lymphocyte antigen-positive skin homing T cells in patients with atopic dermatitis, J. Allergy Clin. Immunol. 117 (2006) 418–425.
[11] A. Takaoka, I. Arai, M. Sugimoto, Y. Honma, N. Futaki, A. Nakamura, S. Nakaike, Involvement of IL-31 on scratching behavior in NC/Nga mice with atopic-like dermatitis, Exp. Dermatol. 15 (2006) 161–167.
[12] U.K. Laemmli, Cleavage of structural proteins during the assembly of the head of bacteriophage T4, Nature 227 (1970) 680–685.
[13] H. Towbin, T. Staehelin, J. Gordon, Electrophoretic transfer of proteins from polyacrylamide gels to nitrocellulose sheets: procedure and some applications, Proc. Natl. Acad. Sci. USA 76 (1979) 4350–4354.
[14] K. Nakai, M. Kanehisa, Prediction of in-vivo modification sites of proteins from their primary structures, J. Biochem. 104 (1988) 693–699.
[15] F. Altmann, S. Schweiszer, C. Weber, Kinetic comparison of peptide: *N*-glycosidases F and A reveals several differences in substrate specificity, Glycoconj. J. 12 (1995) 84–93.

[16] N.S. Seo, A.M. Hocking, M. Hook, D.J. McQuillan, Decorin core protein secretion is regulated by N-linked oligosaccharide, glycosaminoglycan additions, J. Biol. Chem. 280 (2005) 42774–42784.
[17] G.C. Miller, C.J. Long, E.D. Bojilova, D. Marchadier, K.O. Badellino, N. Blanchard, I.V. Fuki, J.M. Glick, D.J. Rader, Role of N-linked glycosylation in the secretion and activity of endothelial lipase, J. Lipid Res. 45 (2004) 2080–2087.
[18] P. Scheiffele, J. Peranen, K. Simons, *N*-Glycans as apical sorting signals in epithelial cells, Nature 378 (1995) 96–98.
[19] H. Liu, J. Yang, J.G. Ling, K.C. Chou, Prediction of protein signal sequences, their cleavage sites by statistical rulers, Biochem. Biophys. Res. Commun. 338 (2005) 1005–1011.
[20] T. Thompson, C. Tovar, H. Yang, D. Carvajal, B.T. Vu, Q. Xu, G.M. Wahl, D.C. Heimbrook, L.T. Vassilev, Phosphorylation of p53 on key serines is dispensable for transcriptional activation and apoptosis, J. Biol. Chem. 279 (2004) 53015–53022.
[21] A.M. Miller, D. Xu, D.L. Asquith, L. Denby, Y. Li, N. Sattar, A.H. Baker, I.B. McInnes, F.Y. Liew, IL-33 reduces the development of atherosclerosis, J. Exp. Med. 205 (2008) 339–346.
[22] J. Schmitz, A. Owyang, E. Oldham, Y. Song, E. Murphy, T.K. McClanahan, G. Zurawski, M. Moshrefi, J. Qin, X. Li, D.M. Gorman, J.F. Bazan, R.A. Kastelein, IL-33, an interleukin-1-like cytokine that signals via the IL-1 receptor-related protein ST2 and induces T helper type 2-associated cytokines, Immunity 23 (2005) 479–490.
[23] W. Nickel, Unconventional secretory routes: Direct protein export across the plasma membrane of mammalian cells, Traffic 6 (2005) 607–614.
[24] F. Tarantini, I. Micucci, S. Bellum, M. Landriscina, S. Garfinkel, I. Prudovsky, T. Maciag, The precursor but not the mature form of IL1alpha blocks the release of FGF1 in response to heat shock, J. Biol. Chem. 276 (2001) 5147–5151.
[25] S. Ponnambalam, S.A. Baldwin, Constitutive protein secretion from the trans-golgi network to the plasma membrane, Mol. Membr. Biol. 20 (2003) 129–139.
[26] G. Jovcic, D. Bugarski, A. Krstic, M. Vlaski, M. Petakov, S. Mojsilovic, N. Stojanovic, P. Milenkovic, The effect of interleukin-17 on hematopoietic cells and cytokine release in mouse spleen, Physiol. Res. 56 (2007) 331–339.
[27] L. Borish, A. Aarons, J. Rumbyrt, P. Cvietusa, J. Negri, S. Wenzel, Interleukin-10 regulation in normal subjects and patients with asthma, J. Allergy Clin. Immunol. 97 (1996) 1288–1296.
[28] B. Foss, E. Ulvestad, O. Bruserud, Platelet-derived growth factor (PDGF) in human acute myelogenous leukemia: PDGF receptor expression, endogenous PDGF release and responsiveness to exogenous PDGF isoforms by in vitro cultured acute myelogenous leukemia blasts, Eur. J. Haematol. 67 (2001) 267–278.
[29] R.J. Webb, J.D. Judah, L.C. Lo, G.M. Thomas, Constitutive secretion of serum albumin requires reversible protein tyrosine phosphorylation events in trans-golgi, Am. J. Physiol. Cell. Physiol. 289 (2005) C748–C756.
[30] T.A. Slimane, C. Lenoir, C. Sapin, M. Maurice, G. Trugnan, Apical secretion and sialylation of soluble dipeptidyl peptidase IV are two related events, Exp. Cell Res. 258 (2000) 184–194.
[31] C.J. Tifft, R.L. Proia, R.D. Camerini-Otero, The folding and cell surface expression of CD4 requires glycosylation, J. Biol. Chem. 267 (1992) 3268–3273.

ANTICANCER RESEARCH *29*: 235-242 (2009)

Application of Therapeutic Insonation to Malignant Glioma Cells and Facilitation by Echo-contrast Microbubbles of Levovist

YOSHINOBU MANOME[1], HIROSHI FURUHATA[2], AKIFUMI HASHIMOTO[1], NAOTAKE FUNAMIZU[1], RIE SUZUKI[1], SHO ISHIZAWA[1], NOBUTAKE AKIYAMA[3], TOSHIAKI KOBAYASHI[4] and MICHIKO WATANABE[1]

Departments of [1]Molecular Cell Biology, [3]Molecular Immunology, Institute of DNA Medicine, Research Center for Medical Sciences and [2]Medical Engineering Laboratory, Research Center for Medical Sciences, Jikei University School of Medicine, Minato-ku, Tokyo 105-8461; [4]Cancer Screening Technology Division, Research Center for Cancer Prevention and Screening, National Cancer Center, Chuo-ku, Tokyo 105-0045, Japan

Abstract. *Background: Malignancies affecting the central nervous system are intractable to conventional therapies thereby requiring an alternative strategy, such as ultrasound irradiation. Materials and Methods: We originally designed a transducer for intracranial insonation and investigated the effect of 210.4 kHz ultrasound on malignant glioma cells. Results: The insonation of 2.61 W/cm^2 effectively disrupted the malignant cells. This effect was reinforced by the echo-contrast agent, Levovist. The condition was applied to tumor-bearing animals and external insonation inhibited subcutaneous tumor growth. It also repressed the growth of intracranially implanted tumors and prolonged survival of the animals. When Levovist was stereotactically injected into the tumors, the effect of insonation was significantly enhanced. Conclusion: A neuronavigation system or stereotactic device has been used commonly for patients with brain tumor. Administration of combination therapy consisting of insonation and a local echo-contrast agent will have a role in improving the treatment for malignant gliomas.*

Malignant glioma is the most common primary tumor in the central nervous system. Since the central nervous system is a critical organ, total resection of the tumor is often difficult. In such cases, a residual tumor recurs and the prognosis for recovery is poor because of the infiltrating nature of the tumor growth. Despite recent advances in adjuvant therapies, tumors still resist various therapies and, therefore, the development of an alternative therapy is required. In this study aimed at utilizing ultrasound, we created an ultrasound transducer for the central nervous system and applied it for the treatment of malignant glioma.

Ultrasound has been commonly used in the clinical field as a diagnostic tool. Compared to other diagnostic equipment, ultrasonic devices are handy and less costly. In addition, they do not emit radiation, making them suitable for non-invasive screening for lesions of superficial organs. They are not only used to observe organs by brightness or the B-mode, but also for dynamic studies, such as the measurement of blood flow or cardiac movement. Other applications of elastography, color Doppler, and 3D sonography are possible. To date, ultrasound has been used widely in the clinical field and many physicians and medical staff are familiar with the technology. The existence of many people who are aware of ultrasound properties is a great advantage for further development and widespread use of treatment using ultrasound.

While ultrasound has long been used as a diagnostic tool, therapeutic applications also have been spotlighted. Several such applications are already commercially available. High-intensity focused ultrasound is a typical example.

High-intensity focused ultrasound (HIFU) is used to treat malignancies such as prostate, uterine, or breast carcinoma. By focusing the high-intensity ultrasound beam onto the lesion, the acoustic force of the ultrasound delivers lethal energy to the tumor tissues. Another application is sonodynamic therapy, which is used for neovascularization and malignancies. By exposure to

Correspondence to: Yoshinobu Manome, MD, Ph.D., Department of Molecular Cell Biology, Institute of DNA Medicine, Research Center for Medical Sciences, Jikei University School of Medicine, 3-25-8 Nishishinbashi, Minato-ku, Tokyo, 105-8461, Japan. Tel: +81 334331111 ext. 2360, e-mail: manome@jikei.ac.jp

Key Words: Ultrasound, echo-contrast agent, microbubbles, malignant glioma, central nervous system.

ultrasound after the administration of a sonosensitizing agent, only neosynthesized blood vessels or malignant cells that accumulate the agent are eliminated by the energy.

Previously, we investigated sonoporation as a therapeutic application of ultrasound and found a favorable effect on gene transfer for colon cancer (1), and on the central nervous system (2). The effect was enhanced by echo-contrast microbubbles. In the context of these experiments, we noticed that the combination of ultrasound and the echo-contrast agent, Levovist, could generate lethal energy to kill intracranial malignant glioma cells by perforating their cell membrane.

Several effects have been demonstrated in the combination of echo-contrast microbubbles and ultrasound (3-9). During insonation, microbubbles absorb physical energy and confer cavitation damage, sonochemistry and sonoluminescence to the neighboring structures. Other than gene transfer, this effect has been applied to drug delivery and thrombolysis (10-15). However, its actual application in clinical fields is relatively limited. The innate cavitation perforates the cellular membrane adjoining ruptured microbubbles and can cause cell death of the surrounding tissue. Ultrasound-induced apoptosis and cell lysis by echo-contrast agents for malignant cells is promising for future cancer therapy (16). Several issues including target tissues, ultrasound devices and conditions need to be addressed before development of clinical therapy by insonation for malignant diseases.

In the current paper, we propose therapeutic ultrasound irradiation for malignant glioma in combination with intratumoral or stereotactic injection of echo-contrast microbubbles. The ultrasonic condition was originally determined during *in vitro* three-dimensional cell culture experiments and applied to tumor-bearing animal models.

Materials and Methods

Insonation. Ultrasound was generated by the wave synthesizer, Wave Factory WF 1943 (NF electronic instruments, Yokohama, Japan). The amplifier and ultrasound probe were produced by Honda Electric Inc., Toyohashi, Japan. The transducer was made of piezo ceramics and the diameter of the probe was 5 mm. This apparatus can emit a continuous wave of 210.4 kHz ultrasound up to 5.08 W/cm^2 measured by the force balance method in water using an ultrasound power meter (UPM-DT-1; Ohmic Instruments Co., Easton, MD, USA). The power intensity of 2.61 W/cm^2 was selected for the study. The reason for this was that, unlike 3.80 W/cm^2, this value was not directly toxic to brain culture slices even for 20 seconds without microbubbles (2). In this setting, the ultrasound intensity of 2.61 W/cm^2 corresponded to 0.143 MPa.

In vitro three-dimensional cell culture of human brain tumor cells. Cells of the human malignant glioma cell line, T98G (ATCC, Rockville, MD, USA), were cultivated in Dulbecco's minimal essential medium supplemented with 10% fetal bovine serum. Cells were grown in a normal culture flask until the start of the experiments. Material for the scaffold of the three-dimensional cell culture was gelatin. The three-dimensional culture method has been described elsewhere (17). In brief, a gelatin sponge was cut into 5-mm cubes and dispersed cells (1×10^4 cells/100 μl) were injected into the sponge. After adhesion of the cells to the scaffold, cubes containing brain tumor cells were transferred into a 10-cm dish and further cultivated at 37°C in a 5% CO_2 incubator for 10 days. Levovist was purchased from Japan Schering, Osaka, Japan. Disruption of the cell membrane by insonation was measured by a chromate-releasing assay.

Chromate-releasing assay. Cells in the three-dimensional cube were labeled with 300 μCi of ^{51}Cr-sodium chromate in 3 ml of culture medium for 4 hours at 37°C in a 5% CO_2 incubator. After three-washes with phosphate-buffered saline (PBS) or by changing the buffers, the cube was insonated with 2.61 W/cm^2 of power intensity (Figure 1). Proportions of the dead cells showing membrane disruption were determined from counts of chromate released into the culture supernatant. Before and after insonation, released radioisotopes were measured and after the experiments, total labeled chromates were measured after cell lysis by adding Triton®X to the inner chamber. Percentage cell death was calculated by dividing the net amount of released chromate by the total amount of labeled chromate ×100.

Animal studies. Four-week-old (50-70 g) of female Fischer 344 rats were purchased from Sankyo Labo-service (Tokyo, Japan). All the animal experiments were performed with permission from the Animal Care Committee at Jikei University School of Medicine. The RT2 glioblastoma cells (18) of 2×10^6 cells/100 μl were implanted subcutaneously into the right flank of syngeneic Fischer 344 rats and then three days later, the rats were treated by insonation and microbubbles for 3 consecutive days. The efficacy of the treatment was assessed from the tumor growth rate.

In another experiment, RT2 cells were implanted stereotactically into the right caudate nucleus using a modification of the method of Kobayashi *et al.* (19). Four-week-old Fischer 344 rats were anesthetized and placed in a small animal stereotactic frame (David Kopf Instruments, Tujunga, CA, USA). A sagittal incision was made through the scalp to expose the skull and a small burr hole was made 1.3 mm posterior and 4 mm lateral to the right of the bregma. Ten thousand tumor cells suspended in 10 μl of PBS were injected with a 701 Hamilton syringe over 30 seconds to a depth of 4.5 mm. The needle was left in place for one minute and withdrawn slowly. The hole in the skull was plugged with bone wax and the incision was closed by surgical clips (Autoclip, 9 mm; Nippon Beckton Dickinson, Tokyo, Japan) (20, 21). On the following day, the rats were treated by insonation. When microbubbles were used, 5 mg in 10 μl of microbubbles were gently injected into the tumor through the needle track using the same stereotactic frame. The tip of the ultrasound beam was adjusted to the tumor-injected site and insonation was conducted through the skull. Rats were treated for 20 seconds for 3 consecutive days and their survival was monitored.

Statistical analysis. Statistical analysis was performed with two-sample *t*-tests. Significance was determined at *p*-values less than the 0.05 level. Statistics were computed using the Statview statistic package (ver. 5.0: SAS Institute Inc, Berkeley, CA, USA).

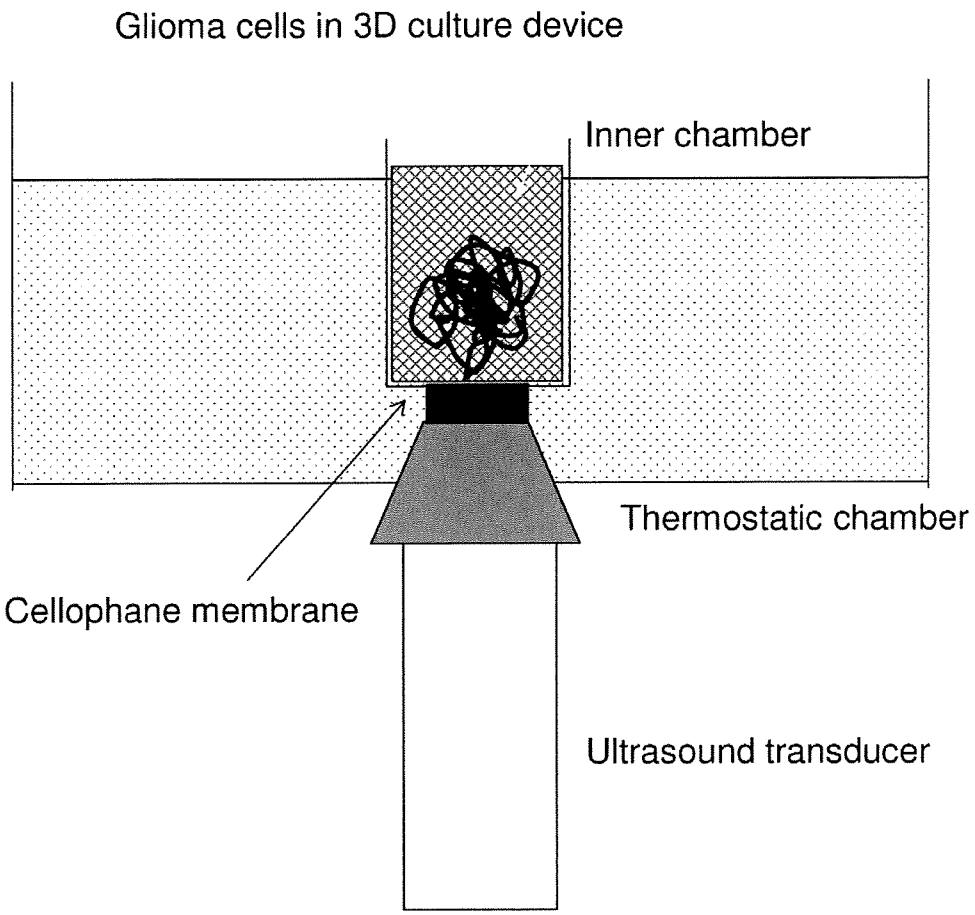

Figure 1. *In vitro experiment of insonation with three-dimensional culture cells. Three-dimensionally cultured cells were radio-labeled with sodium chromate for 4 hours. After washing, cells in a sponge were directly insonated with or without microbubbles through the bottom of the cellophane membrane of the inner chamber. The chromate released by insonation was determined and the proportion of dead cells with membrane disintegration was calculated.*

Results

Insonation disrupts the cell membrane by cavitation. Previously, we used 210.4 kHz of ultrasound and observed membrane disintegration of cells of the central nervous system by scanning electron microscopy (2). To confirm if insonation could induce cell membrane porosity in glioma cells with microbubbles of the echo-contrast agent, Levovist, the effect on cell viability was evaluated as the first step of the experiments. Three-dimensionally cultured glioma cells were insonated at 2.61 W/cm^2 with 30 mg/ml of Levovist. The membrane integrity was assayed by chromate-releasing assay. Unless insonation was performed, there was barely any chromate released from the cells. Insonation disrupted the cell membrane and chromate was released into the culture supernatant. When the insonation time was extended, cell death as shown by chromate release also increased (Figure 2A). Since the ultrasound power intensity was constant, time elongation meant an increase in the total dose of insonation. As the insonation time was doubled, the amount of chromate released was approximately doubled. There was a direct correlation between cell death defined by the release of chromate and the duration of insonation in the range of 0 to 40 seconds.

In order to determine whether microbubbles could modify membrane disintegration, the dose effect of the microbubbles was examined. Cells were exposed to several dilutions of microbubbles and insonated at 2.61 W/cm^2 for 20 seconds. The amount of chromate released under each condition was measured and the effect of the microbubbles determined. When the concentration of microbubbles increased, cell death also increased (Figure 2B). However, the correlation was not proportional. Cell death at 60 mg/ml was less than twice that at 30 mg/ml of microbubbles. Additionally, the effect almost plateaued at concentrations above 60 mg/ml.

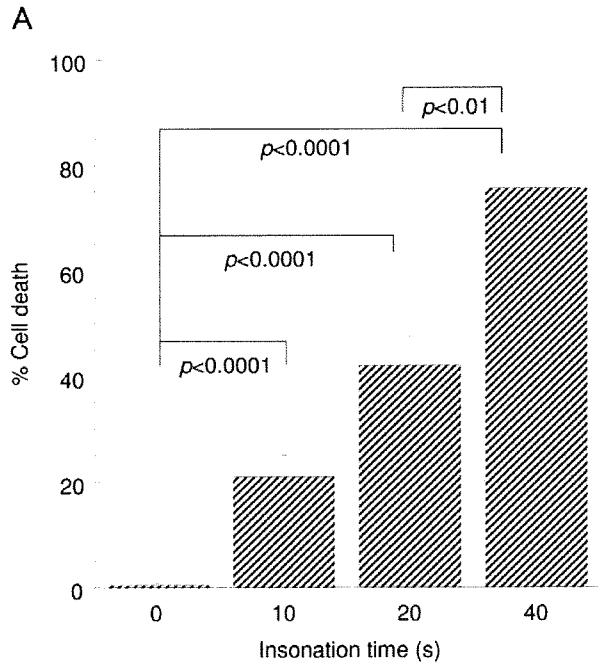

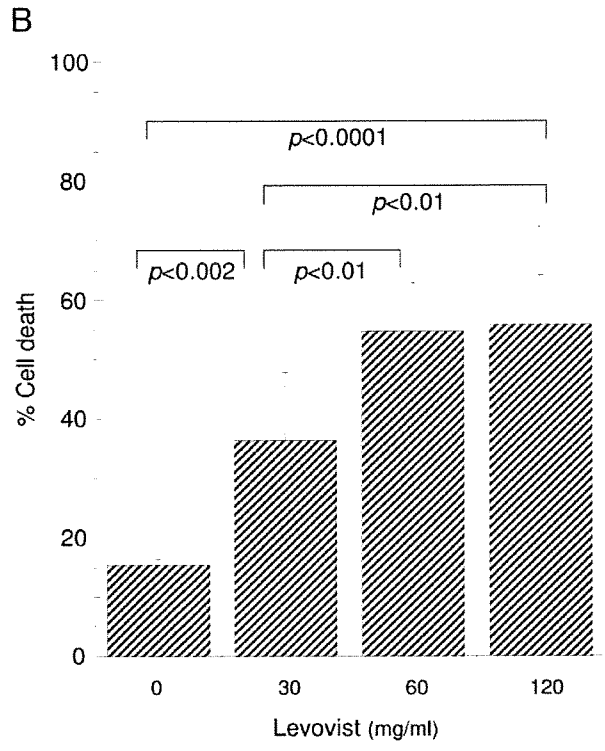

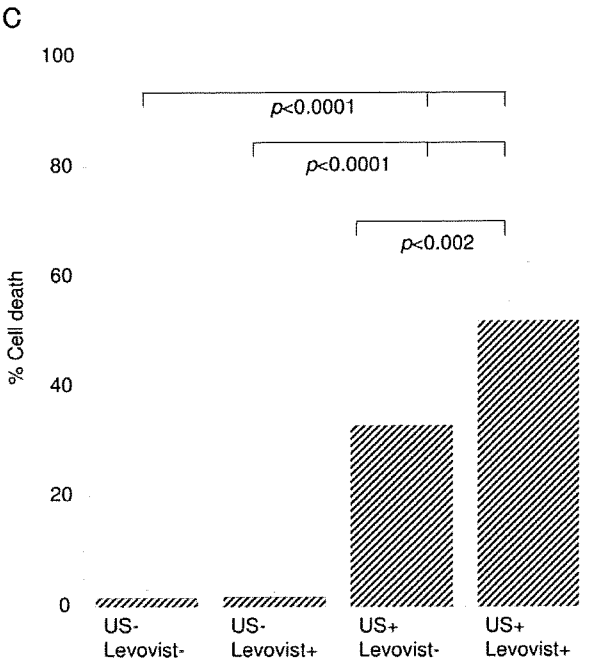

Figure 2. *Effect of ultrasound on glioma cell death. A. Relationship of insonation time to cell death. Glioma cells in three-dimensional culture were irradiated with various durations of insonation. Within the measured ranges, the percentage of dead cells increased when the insonation time was elongated. Note that since the power intensity of the ultrasound was constant 2.61W/ cm^2, the total dose of acoustic energy increased when the insonation time was extended. Results are expressed as the mean of six experiments and the bars indicate sample standard deviation. B. Relationship of Levovist concentration to cell death. Glioma cells were irradiated with various concentrations of Levovist. Ultrasound of 2.61 W/cm^2 for 20 seconds was used in the experiment. A correlation was seen between a low concentration of microbubbles and the amount of cell death. However at higher concentrations, the effect plateaued. Results are expressed as the mean of six experiments and the bars indicate sample standard deviation. C. Effect of the combination of insonation and Levovist on cell death. Glioma cells were treated or not treated with ultrasound and Levovist. Conditions of the ultrasound were 2.61 W/cm^2 for 0 (US–) and 20 seconds (US+ Levovist+). The concentration of Levovist was 0 (Levovist–) and 30 mg/ml. Levovist by itself did not confer toxicity on the cells. On the contrary, insonation alone caused chromate release. The effect was significantly enhanced by Levovist. Results are expressed as the mean of six experiments and the bars indicate the sample standard deviation.*

In these experiments, insonation induced chromate release and a low concentration, in the range of 0 to 60 mg/ml, of microbubbles facilitated the effect. To validate the effect of insonation and microbubbles, cells were treated with 0 or 30 mg/ml of microbubbles and insonation at 0 or 2.61 W/cm^2 for 20 seconds and the differences in each group were examined. Unless insonated, the microbubbles themselves led to very little cell death in glioma and there was no difference between the treated and non-treated groups (Figure 2C). When cells were exposed to the ultrasound, insonation caused chromate release under such conditions. Differences were observed between the insonated and non-

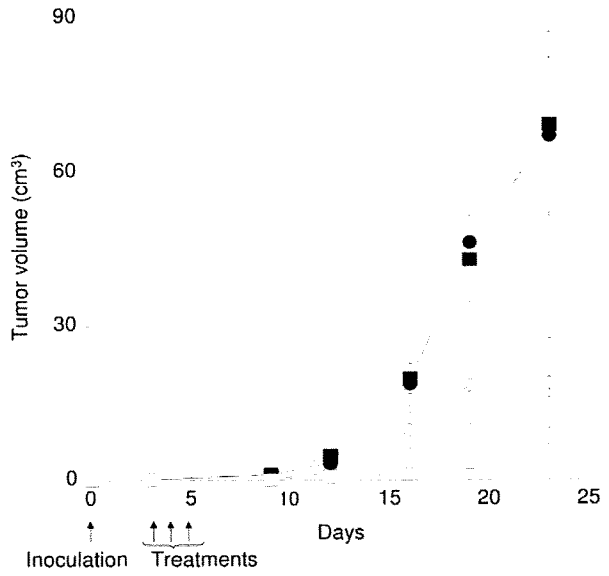

Figure 3. *Tumor growth retardation by insonation. After the inoculation of glioma cells, the subcutaneous tumor nodule was sequentially treated with insonation and Levovist for three days. Rats were treated with 0 seconds of 2.61 W/cm² of insonation with 0 mg/ml of Levovist (●), 0 seconds of insonation with 30 mg/ml of Levovist (■), 20 seconds of insonation with 0 mg/ml of Levovist (○), and 20 seconds of insonation with 30 mg/ml of Levovist (□). Results are expressed as the mean of each rat and the bars indicate sample standard deviation.*

insonated groups ($p<0.0001$) as previously suggested. When cells were treated with microbubbles, presence of the echo-contrast agent enhanced cell death by ultrasound. Under ultrasound exposure, there was a difference in the death of cells treated with microbubbles and those without them ($p<0.002$).

The results of the *in vitro* studies suggested a potential application of insonation in oncotherapy for brain tumor. Efficacy of the treatment was successively examined by *in vivo* experiments. RT2 glioma cells were implanted into the right flank of Fischer 344 rats. After confirmation that a small tumor nodule was established at the implanted site, the rats were treated with local microbubble injection followed by insonation for three days. When the rats were treated only by microbubbles and not insonated, the growth of the tumor was almost equal to that of the untreated control rats (Figure 3.) In contrast, ultrasound exposure inhibited tumor growth. The effect was significantly enhanced by co-treatment with microbubbles ($p<0.01$ day 9, 12, 16, and $p<0.05$ day 19). Unlike the other groups, the combination of insonation and microbubbles even led to a cure in some animals. Three out of six rats treated by insonation with microbubbles demonstrated complete tumor regression. These rats survived for more than 365 days without any recurrence.

Since combination treatment was effective for *in vivo* malignant glioma, tumor cells were stereotactically inoculated into the caudate nucleus of brain parenchyma and then the efficacy of treatment was evaluated. After implantation of RT2 glioma cells, rats were treated by insonation with or without echo-contrast microbubbles. As a control, other rats were mock insonated. Due to limited intracranial space and rapid growth of the tumor, the animals had a low survival. All the rats died by day 15 unless insonated, whether with or without microbubbles (Figure 4). Mean survival was 12.62±1.84 days for untreated animals, and 12.13±1.13 days for animals treated with microbubbles. When the rats were insonated, the treatment prolonged their survival (mean survival: 15.50±4.04 days). The effect was further reinforced by microbubbles (mean survival: 20.71±3.04 days). There were significant differences between the untreated group or that treated only by microbubbles and the group treated with both insonation and microbubbles (p-values <0.0001).

Discussion

Malignant glioma is one of the most intractable diseases in the human body. In spite of recent advancements of therapies, including surgery, radiotherapy, chemotherapy, immunotherapy and other adjuvant therapies, this disease is refractory and the prognosis is unsatisfactory, with median survival times of 5.6 years for low-grade astrocytoma, 1.6 years for anaplastic astrocytoma and 0.4 years for glioblastoma, respectively (22). Since most patients die within 2 to 5 years after their diagnosis and the efficacy of current therapy is limited, a potent alternative strategy is required. In spite of poor patient prognosis, the tumor seldom metastasizes to organs other than the central nervous system and since the main cause of death is local recurrence of the tumor, long-term survival or even complete remission can be expected only by modulation of local recurrence (23). In addition, a direct route for drug or material delivery into the tumor is available (24). The advantage of the central nervous system for developing a new therapy is that agents can be administered into brain parenchyma by stereotactic surgery, neuronavigation or utilization of the Ommaya reservoir. These methods have been commonly used as clinical procedures and lesions are accessible by these methods.

As a therapeutic tool, ultrasound has been highlighted since it induces cell membrane porosity (25). The impact of ultrasonic forces also induces mechanical damage to living tissues, stones, clots, or other organic and inorganic compounds. It has the capability for transmitting mechanical power or force to a distant area of the human body, therefore insonation can be applied not only to the superficial tissues, but also to deeper areas. Compared to therapies with energies of shorter wavelength, such as photons, this may be a benefit

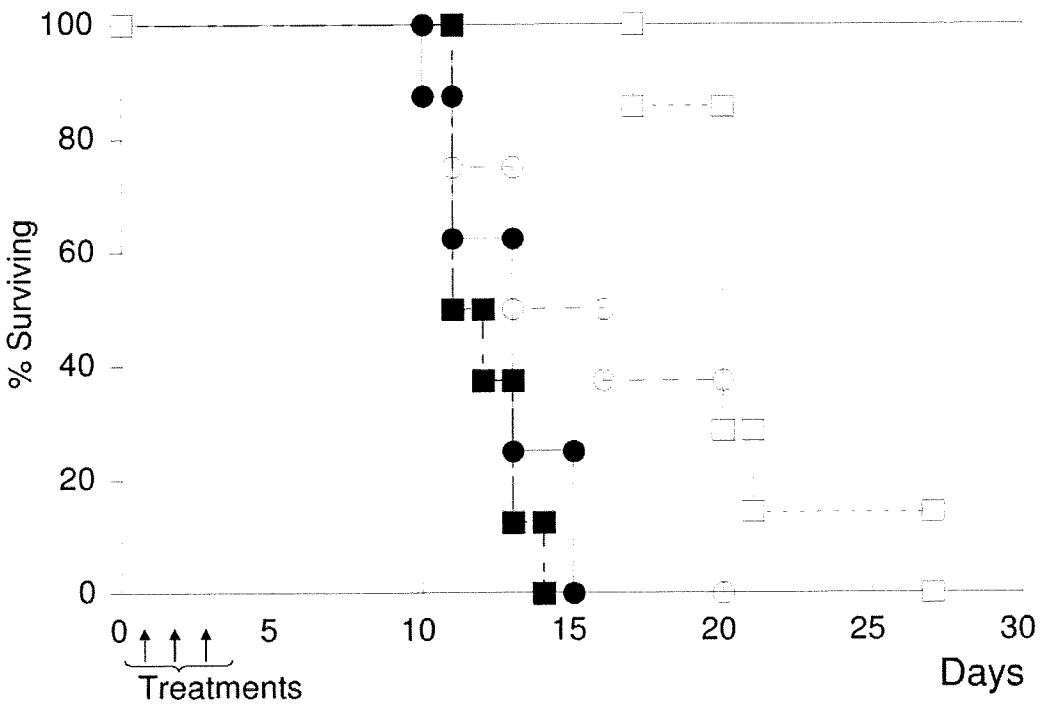

Figure 4. *Therapeutic efficacy of insonation to intracerebral tumor. Therapeutic efficacy of insonation was evaluated by survival of the tumor-bearing animals. After stereotactic inoculation of glioma cells into the caudate nucleus of the right cerebrum, the animals were treated with local administration of Levovist and external insonation. Rats were treated with 0 seconds of 2.61 W/cm² of insonation with 0 mg of Levovist (●), 0 seconds of insonation with 3 mg of Levovist (■), 20 seconds of insonation with 0 mg of Levovist (○), and 20 seconds of insonation with 3 mg of Levovist (□). Results are expressed as the mean of 8 individuals and the bars indicate sample standard deviation.*

for the treatment of deep-seated lesions. Brain tumor is one of the most suitable targets for the application of insonation.

Ultrasound with a continuous 210.4 kHz wave was used for the study. The reason for this was based on a previous finding that ultrasound with this frequency could perforate the cell membrane of central nervous glial cells effectively (2). Perforation of the cell membrane was observed by scanning electron microscopy. The effect was similar to that demonstrated by Tachibana *et al.* (25). The mechanical index of the current study was 0.32, which is less than 0.612 of a previous gene delivery study for neonatal glial cells that was also conducted at 210.4 kHz. Furthermore, for gene delivery, unlike the power intensity of 2.61 W/cm^2 used in the current study, 5.0 W/cm^2 was required to transduce DNA by ultrasound for gene expression, since DNA had to be delivered into the cell nucleus across cellular and nuclear membranes. In addition to the macromolecular nature of DNA, both the cell membrane and DNA were positively charged and electrically repelled. Therefore, a higher external force was required for gene transduction. Correspondingly, the thermal index category soft tissue, or TIS, was smaller (=0.489) than that of the previous study (=0.935). In the experiments, employment of microbubbles enabled further energy to reach the local area of the insonation field.

Kudo *et al.* reported that microbubbles exposed to ultrasound caused mechanical stress that acted on the cells and bubble collapse was responsible for cell membrane damage (6). Even gentle linear bubble oscillation is sufficient to achieve rupture of lipid membranes (9). Currently, air-filled albumin microspheres (Albunex), non-shell type granules composed of 99.9% galactose and 0.1% palmitic acid (Levovist), and an albumin-shelled agent composed of fluorocarbon gas octafluoropropane (Optison) have been used as echo-contrast agents in the clinical field. In this study, we tested Levovist, which is the only agent available in Japan. As the next step, a comparison of microbubbles will be required in order to optimize the combination.

The effect of ultrasound was first evaluated on three-dimensionally cultured glioma cells and then applied to *in vivo* studies. This approach was useful for the study since the effects evaluated by two-dimensional culture did not correlate with those obtained with animals. Aside from cell detachments from the flat and hard plastic or plastic substrate

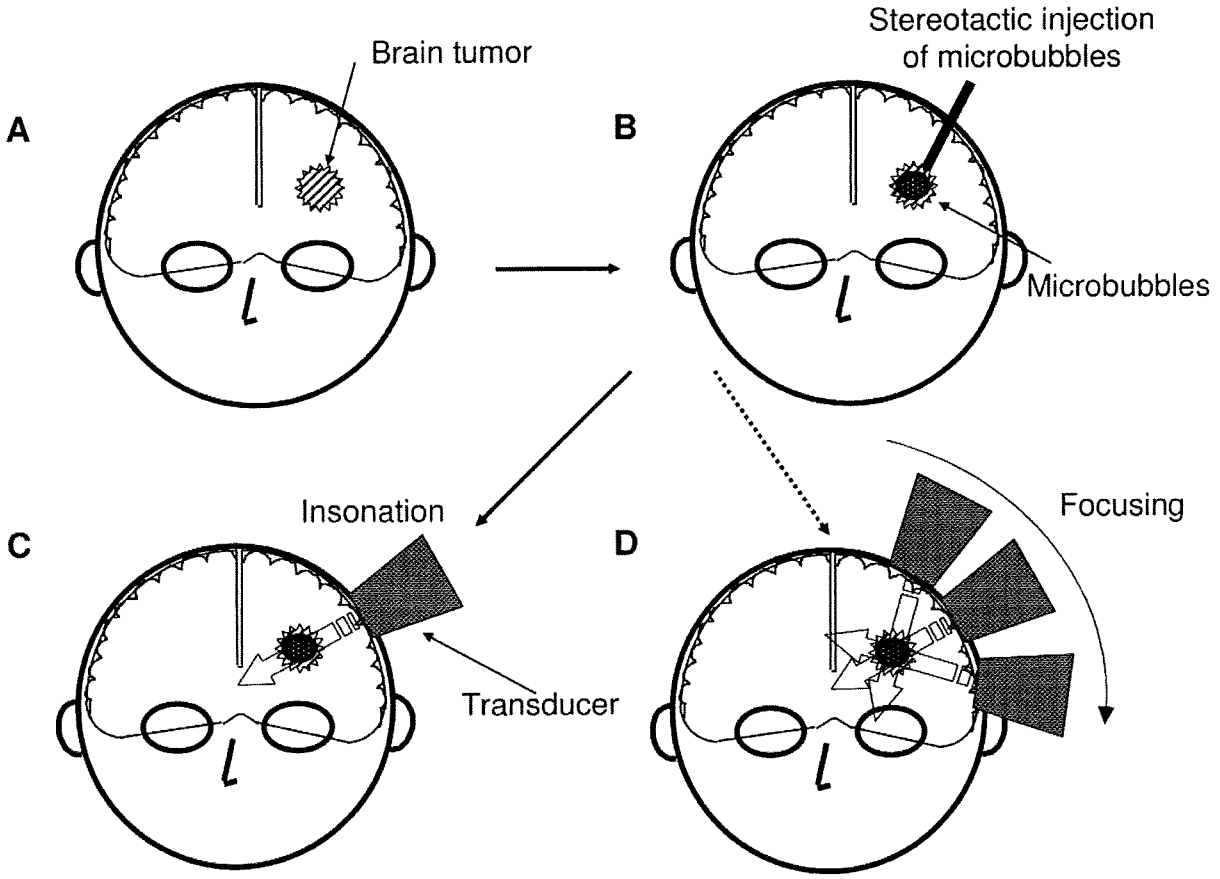

Figure 5. *Schema of a possible approach to malignant glioma using intratumoral injection of microbubbles and insonation. A, When a patient is examined, medical imaging instruments show the location and size of the tumor. The patient undergoes treatment. B, Stereotactic injection of microbubbles into an intracranial tumor results in increased sensitivity of ultrasound and glioma cells become vulnerable to the ultrasound. C, External insonation of the injected site induces cell death in the tumor tissue. Although the power level of ultrasound is attenuated during passage through the cranium, insonation with 210.4 kHz transmits sufficient intensity to the deep area of the cerebrum. D, One of the characteristics of insonation is accumulation of acoustic energy in the insonated region. Ultrasound can be focused by moving the tip of the transducer of ultrasound and, by so doing, the conduction effect can be intensified without damaging unfocused areas of the brain.*

caused by insonation, ordinary cell culture generally did not present tissue-specific architecture, mechanical and biochemical cues or cell-to-cell communication and did not mimic the function of living tissues (26). While the quantitative analysis method as well as scaffold materials and pore sizes needed to be more sophisticated, the results obtained in the three-dimensional cell culture were comparable to the results of animal experiments.

The authors previously implanted a malignant brain tumor in the caudate nucleus of the cerebrum of rats, injected drugs or adenoviral vectors encoding β-galactosidase with a stereotactic device and found that agents can be delivered to the center of implanted brain tumor (18, 21, 27). One possible application of the strategy is shown in Figure 5. By focusing the ultrasound, intensified power energy can be concentrated on the target area. This possibility is valuable for such a therapeutic approach.

HIFU has been recently highlighted for the treatment of malignant tumors. The difference from our method is in the power intensity of the emission ultrasound. Echo-contrast agent, such as Levovist, oscillate by insonation and rupture due to inert cavitation. In this step, intense heat and mechanical forces are produced at the ruptured site. In combination to an echo-contrast agent, ultrasound can generate enough power to eradicate malignant glioma cells. For treatment of the central nervous system, avoiding the adverse effect of therapy is essential since the central nervous system is critical, as once neuronal cells are

damaged, they seldom regenerate. The power intensity used in the present study was extraordinarily less than that of HIFU. Even though a lower intensity is set for the unfocused area of HIFU, utilizing as low an intensity as possible is desirable for treatment of intracranial lesions. Our previous toxicity study demonstrated minimal invasiveness to the central nervous system cells (2).

We have demonstrated therapeutic ultrasound irradiation for malignant glioma in combination with stereotactic intratumoral injection of echo-contrast microbubbles. The ultrasonic condition used for the study might have clinical relevancy. Further study is warranted.

References

1 Manome Y, Nakamura M, Ohno T and Furuhata H: Ultrasound facilitates transduction of naked plasmid DNA into colon carcinoma cells *in vitro* and *in vivo*. Hum Gene Ther *11*: 1521-1528, 2000.

2 Manome Y, Nakayama N, Nakayama K and Furuhata H: Insonation facilitates plasmid DNA transfection into the central nervous system and microbubbles enhance the effect. Ultrasound Med Biol *31*: 693-702, 2005.

3 Unger EC, Hersh E, Vannan M and McCreery T: Gene delivery using ultrasound contrast agents. Echocardiography *18*: 355-361, 2001.

4 Unger EC, Hersh E, Vannan M, Matsunaga TO and McCreery T: Local drug and gene delivery through microbubbles. Prog Cardiovasc Dis *44*: 45-54, 2001.

5 Luo W, Zhou X, Tian X, Ren, X, Zheng M, Gu K and He G: Enhancement of ultrasound contrast agent in high-intensity focused ultrasound ablation. Adv Ther *23*: 861-868, 2006.

6 Kudo N, Miyaoka T, Okada K, Yamamoto K and Niwa K: Study on mechanisms of cell damage caused by microbubbles exposed to ultrasound. IEEE Ultrasonics Symp Proc, pp. 1351-1354, 2002.

7 Coussios CC, Farny CH, Haar GT and Roy RA: Role of acoustic cavitation in the delivery and monitoring of cancer treatment by high-intensity focused ultrasound (HIFU). Int J Hyperthermia *23*: 105-120, 2007.

8 Correas JM, Bridal L, Lesavre A, Mejean A, Claudon M and Helenon O: Ultrasound contrast agents: properties, principles of action, tolerance, and artifacts. Eur Radiol *11*: 1316-1328, 2001.

9 Marmottant P and Hilgenfeldt S: Controlled vesicle deformation and lysis by single oscillating bubbles: Nature *423*: 153-156, 2003.

10 Bull JL: The application of microbubbles for targeted drug delivery. Expert Opin Drug Deliv *4*: 475-493, 2007.

11 Postema M and Gilja OH: Ultrasound-directed drug delivery. Curr Pharm Biotechnol *8*: 355-361, 2007.

12 Van Wamel A, Kooiman K and De Jong N: Ultrasound contrast agents pushing drug delivery: high speed optical observations. J Acoust Soc Am *123*: 3215, 2008.

13 Tachibana K and Tachibana S: The use of ultrasound for drug delivery: Echocardiography *18*: 323-328, 2001.

14 Ishibashi T, Akiyama M, Onoue H, Abe T and Furuhata H: Can transcranial ultrasonication increase recanalization flow with tissue plasminogen activator? Stroke *33*: 1399-1404, 2002.

15 Saguchi T, Onoue H, Urashima M, Ishibashi T, Abe T and Furuhata H: Effective and safe conditions of low-frequency transcranial ultrasonic thrombolysis for acute ischemic stroke: neurologic and histologic evaluation in a rat middle cerebral artery stroke model. Stroke *39*: 1007-1011, 2008.

16 Feril LB Jr, Kondo T, Zhao QL, Ogawa R, Tachibana K, Kudo N, Fujimoto S and Nakamura S: Enhancement of ultrasound-induced apoptosis and cell lysis by echo-contrast agents. Ultrasound Med Biol *29*: 331-337, 2003.

17 Manome Y, Saeki N, Yoshinaga H, Watanabe M and Mizuno S: A culture device demonstrates that hydrostatic pressure increases mRNA of RGS5 in neuroblastoma and CHC1-L in lymphocytic cells. Cells Tissues Organs *174*: 155-161, 2003.

18 Parr MJ, Manome Y, Tanaka T, Wen P, Kufe DW, Kaelin WG, Jr., and Fine HA: Tumor-selective transgene expression *in vivo* mediated by an E2F-responsive adenoviral vector. Nat Med *3*: 1145-1149, 1997.

19 Kobayashi N, Allen N, Clendenon NR and Ko LW: An improved rat brain-tumor model. J Neurosurg *53*: 808-815, 1980.

20 Manome Y, Watanabe M, Futaki K, Ishiguro H, Iwagami S, Noda K, Dobashi H, Ochiai Y, Ohara Y, Sanuki K, Kunieda T and Ohno T: Development of a syngenic brain-tumor model resistant to chloroethyl-nitrosourea using a methylguanine DNA methyltransferase cDNA. Anticancer Res *19*: 5313-5318, 1999.

21 Manome Y, Watanabe M, Abe T, Tomita M, Watanabe S, Yokokawa Y, Takahashi Y, Ishii K, Kimura A, Murakami M Nagata M, Shibata T, Nakamura M, Tanigawa N and Ohno T: Transduction of thymidine phosphorylase cDNA facilitates efficacy of cytosine deaminase/5-FC gene therapy for malignant brain tumor. Anticancer Res *21*: 2265-2272, 2001.

22 Ohgaki H and Kleihues P: Population-based studies on incidence, survival rates, and genetic alterations in astrocytic and oligodendroglial gliomas. J Neuropathol Exp Neurol *64*: 479-489, 2005.

23 Manome Y, Kobayashi T, Mori M, Suzuki R, Funamizu N, Akiyama N, Inoue S, Tabata Y and Watanabe M: Local delivery of doxorubicin for malignant glioma by a biodegradable PLGA polymer sheet. Anticancer Res *26*: 3317-3326, 2006.

24 Manome Y, Kunieda T, Wen PY, Koga T, Kufe DW and Ohno T: Transgene expression in malignant glioma using a replication-defective adenoviral vector containing the Egr-1 promoter: activation by ionizing radiation or uptake of radioactive iododeoxyuridine. Hum Gene Ther *9*: 1409-1417, 1998.

25 Tachibana K, Uchida T, Ogawa K, Yamashita N and Tamura K: Induction of cell-membrane porosity by ultrasound. Lancet *353*: 1409, 1999.

26 Pampaloni F, Reynaud EG and Stelzer EH: The third dimension bridges the gap between cell culture and live tissue. Nat Rev Mol Cell Biol *8*: 839-845, 2007.

27 Manome Y, Wen PY, Dong Y, Tanaka T, Mitchell BS, Kufe DW and Fine HA: Viral vector transduction of the human deoxycytidine kinase cDNA sensitizes glioma cells to the cytotoxic effects of cytosine arabinoside *in vitro* and *in vivo*. Nat Med *2*: 567-573, 1996.

Received July 1, 2008
Revised November 18, 2008
Accepted December 1, 2008

IOP PUBLISHING NANOTECHNOLOGY
Nanotechnology 19 (2008) 415102 (7pp) doi:10.1088/0957-4484/19/41/415102

Luminescent passive-oxidized silicon quantum dots as biological staining labels and their cytotoxicity effects at high concentration

Kouki Fujioka[1,2], Masaki Hiruoka[3], Keisuke Sato[3,4], Noriyoshi Manabe[1], Ryosuke Miyasaka[5], Sanshiro Hanada[1], Akiyoshi Hoshino[1], Richard D Tilley[6], Yoshinobu Manome[2], Kenji Hirakuri[3] and Kenji Yamamoto[1,7]

[1] International Clinical Research Centre, Research Institute, International Medical Centre of Japan, Japan
[2] Institute of DNA Medicine, Research Centre for Medical Sciences, Jikei University School of Medicine, Japan
[3] Department of Electronic and Computer Engineering, Tokyo Denki University, Japan
[4] Ion Beam Group, Quantum Beam Centre, National Institute for Materials Science, Ibaraki, Japan
[5] Sangi Corporation Ltd, Japan
[6] MacDiarmid Institute of Advanced Materials and Nanotechnology, Victoria University of Wellington, New Zealand

E-mail: backen@ri.imcj.go.jp (K Yamamoto)

Received 16 June 2008, in final form 30 July 2008
Published 3 September 2008
Online at stacks.iop.org/Nano/19/415102

Abstract
Semiconductor quantum dots (QDs) hold some advantages over conventional organic fluorescent dyes. Due to these advantages, they are becoming increasingly popular in the field of bioimaging. However, recent work suggests that cadmium based QDs affect cellular activity. As a substitute for cadmium based QDs, we have developed photoluminescent stable silicon quantum dots (Si-QDs) with a passive-oxidation technique. Si-QDs (size: 6.5 ± 1.5 nm) emit green light, and they have been used as biological labels for living cell imaging. In order to determine the minimum concentration for cytotoxicity, we investigated the response of HeLa cells. We have shown that the toxicity of Si-QDs was not observed at 112 μg ml^{-1} and that Si-QDs were less toxic than CdSe-QDs at high concentration in mitochondrial assays and with lactate dehydrogenase (LDH) assays. Especially under UV exposure, Si-QDs were more than ten times safer than CdSe-QDs. We suggest that one mechanism for the cytotoxicity is that Si-QDs can generate oxygen radicals and these radicals are associated with membrane damages. This work has demonstrated the suitability of Si-QDs for bioimaging in lower concentration, and their cytotoxicity and one toxicity mechanism at high concentration.

1. Introduction

Semiconductor quantum dots (QDs) hold some advantages over organic fluorescent dyes, including greater fluorescent brightness, photostability, and a wider range of excitation/emission wavelength. Taking advantage of these characteristics, QDs are used as fluorescent labels in many biomedical studies [1–9]. Moreover, QDs are also expected to be applicable for detection systems of small quantity substances on microchips and microarrays [10–14], and in real-time noninvasive detection systems [15, 16].

However, many of the current QDs, most notably CdSe and CdS, contain inherently toxic elements (e.g., cadmium).

[7] Address for correspondence: Director's Laboratory, International Clinical Research Centre of Japan, Research Institute, International Medical Centre of Japan, Toyama 1-21-1, Shinjuku-ku, Tokyo 162-8655, Japan.

Taking toxicological effects on humans and on the environment into consideration, there still remain issues to clear cadmium based QDs for widespread applications. Derfus *et al* have shown that free cadmium ions were released from CdSe-QDs under oxidative condition such as air or exposure to ultraviolet (UV) light and that the cadmium ions induce hepatocyte cytotoxicity *in vitro* [17]. In our recent study, CdSe-QDs affected cell viability in concentrations above 100 μg ml^{-1} without UV exposure [18]. Furthermore, other groups have shown that CdTe-QDs induce toxicological effects *in vitro* [19, 20].

Due to this considerable issue, a shift to safer and more reliable materials will be required for QD applications. Of potential materials, silicon (Si) will be one of the ideal candidates. Luminescent Si quantum dots (Si-QDs) have been studied because of their considerable potential for optoelectronic applications [21, 22] and fluorescent probes for bioimaging [23–25]. Si-QDs, of size less than the bulk exciton Bohr radius of 4 nm, widen the band gap due to quantum confinement [26, 27]. An increase in the photoluminescence (PL) yield along with a shift to the visible spectrum has been observed in Si-QDs [26–30]. Several methods have been developed for producing Si-QDs, including laser pyrolysis [31], aerosols [32], thermal deposition in supercritical solvent [27, 33], plasma deposition [34], electrochemical etching of silicon wafers [35] and colloids [25–27, 29]. Although some Si-QDs have good potential, many of the Si-QDs formed have two problems: (1) stability of PL and the surface state, and (2) lower yields [36]. In order to synthesize stable Si-QDs, Ruckenstein's group has been trying organic capping or graft polymerization [24, 36, 37]. Our previous study showed that water-soluble Si-QDs that have PL stability had a potential use as biological fluorescent labels [25]. However, the low yields, a few mg per batch, prevented further investigation. If Si-QDs can be produced in comparable qualities and quantities, they will have advantages in many applications, especially medical applications and bioimaging, compared to inherently toxic QDs.

Recently, an efficient method for preparing relatively large quantities of brightly luminescent Si-QDs was developed, in which the Si-QDs were formed by radio frequency (RF) sputtering and thermal treatment, and then they were etched with hydrofluoric steam [38]. Some tens of mg per batch were produced in the method. The Si-QDs were water-soluble due to hydroxyl group on their surface [38], and their PL was made stable by oxygen-passivation [39] and could be tuned by controlling the etching time.

Here we present (1) the suitability for bioimaging labels of the oxygen-passivated Si-QDs, (2) cytotoxicity studies of the Si-QDs *in vitro* with and without UV exposure, compared to CdSe-QDs, and (3) a suggestion for the cytotoxicity mechanism of the Si-QDs at high concentration.

2. Experimental details

2.1. Quantum dot synthesis

Silicon quantum dots (Si-QDs) were prepared with the methods described previously [38, 39], and purified with pure water. The photoluminescence spectra of Si-QDs in phosphate buffered saline (PBS) were detected by using a fluorescence spectrometer, FP-6500 (Jasco, Japan). MAA-coated CdSe quantum dots (CdSe-QDs) were produced by replacing the *N*-trioctylphosphine oxide (TOPO) of TOPO-coated QDs by mercaptoacetic acid (MAA) as follows. MAA (Wako Pure Chemical, Japan) in ethanol solution was dropped into the TOPO-coated CdSe-QDs in tetrahydrofuran (Wako Pure Chemicals, Japan). Then the mixture was heated up to 82 °C, and refluxed for 12 h. After the reflux, NaOH solution (pH 10) was added. The mixture was evaporated at 90 °C to remove the tetrahydrofuran. The CdSe-QD solution was purified and concentrated with an ultrafiltration membrane, Microcon Amicon Ultra-4 (Millipore, USA). Additionally, the CdSe-QDs were purified using a gel filtration column (MicroSpin G-25 Columns; GE Healthcare, UK). From dynamic light scattering measurement, the average size of the CdSe-QDs was 5.3 nm (data not shown).

2.2. Electron microscopy investigation

Scanning electron microscopy (SEM) investigations were carried out using a JSM-7500F (JEOL, Japan) electron microscope, operating at an acceleration voltage of 15 kV. High resolution transmission electron microscopy (HRTEM) investigations were carried out using an H-9000 NAR (Hitachi, Japan) electron microscope.

2.3. Fluorescent microscopy analysis

The fluorescent microscopy analysis was performed using an IX81 (Olympus, Japan) fluorescent microscope, attached with a CoolSNAP HQ (Roper Scientific, USA) cooled-CCD camera, and DSU unit (Olympus, Japan). We used human cervical carcinoma cell line, HeLa cells, which were cultured in minimal essential medium alpha (MEM-α; Invitrogen, USA). The cells were cultured on glass-bottom dishes for 48 h at 37 °C/5% CO_2 in the dark. The Si-QDs were added and co-cultured for another 48 h (the final concentration was 56 μg ml^{-1}). After the incubation, the cells were washed with PBS. We detected the green fluorescence of the Si-QDs with the filter sets of an excitation filter 460–480 nm, an absorbance filter 495–540 nm, and a dichroic mirror.

2.4. Cytotoxicity assays

For the cytotoxicity assays, we used HeLa cells and human hepatocytes (Lonza, USA). We cultured 5000 cells (HeLa cells) or 2500 cells (hepatocytes) in each well of 96-well plates for 48 h 37 °C/5% CO_2 in the dark. Then, the Si-QDs or MAA-coated CdSe-QDs were added in indicated concentrations, and co-cultured for 48 h. In order to test the effects of UV exposure, we used QDs exposed to UV light (254 nm) with a power density of 1.8 mW cm^{-2} for 2 h. The cytotoxicities of QDs were examined in two different ways: mitochondrial activity assay and lactate dehydrogenase (LDH) release assay. For the measurement of mitochondrial activity, a Cell Counting Kit-8 (Dojindo, Japan) was used to measure the succinate dehydrogenase mitochondrial activity [40, 41]. The